

Preface

Four Lectures on Elastic Fracture Mechanics

These four lectures were prepared during my sabbatical visit to ESPCI Paris Tech during the months of November 2013 to March 2014. During this time I was supported by Michelin Corporation, by ESPCI and by Total Corporation. The focus of these lectures is on certain fundamental aspects of elastic fracture mechanics that are difficult to find in textbooks. These lectures, two hours each, are given to students and faculties of ESPCI during the month of January 2014. My goal is to make these lectures as self-contained as possible, assuming only basic knowledge of solid mechanics. Some of the materials are taken from papers by James Rice and John Eshelby as well as from the nonlinear fracture mechanics book written by John Hutchinson. The review on large deformation theory in lecture 3 draws heavily from the lecture notes of Tim Healey, who teaches the nonlinear elasticity course in our department.

Finally, I thank Costantino Creton and Matteo Ciccotti for hosting me at ESPCI. Also, since these notes were prepared during a short period of time, I would be very grateful if readers would inform me of any errors which they detect.

Lecture 1 Linear Elastic Fracture Mechanics: Basic Concepts (Small Scale Yielding: SSY)

Notation:

Components of vectors and tensors in 3D are indexed by i, j, k . Components of vectors and tensors in 2D are indexed by Greek letter such as α, β .

Summation convention of summing over repeated indices will be used throughout unless specified otherwise. We denote the position of a material point by its Cartesian coordinates x_i . The notation $,_i$ denotes partial derivative with respect to x_i .

Basic assumption: The solid is homogeneous, isotropic and linearly elastic in Lecture 1 and lecture 2. Small strain theory (where displacements, displacement gradients and rotations are assumed to be small) will be used throughout the first 2 lectures. I limit discussions to quasi-static problems and without loss of generality, assume zero body forces.

Review of Linear Elasticity

The basic equations of linear elasticity are:

The Cartesian component of the symmetric stress tensor σ_{ij} obeys

$$\sigma_{ij,j} = 0 \quad \text{Force balance (no body forces, quasi-static)} \quad (1)$$

The symmetric strain tensor ε_{ij} is related to the displacements of material points by

$$\varepsilon_{ij} = \frac{u_{i,j} + u_{j,i}}{2} \quad \text{Kinematics} \quad (2)$$

Finally, isotropic implies that

$$\varepsilon_{ij} = \frac{(1+\nu)\sigma_{ij}}{E} - \frac{\nu\sigma_{kk}}{E}\delta_{ij} \quad \text{Constitutive model (generalized Hooke's law)} \quad (3)$$

where E is the Young's Modulus and ν is the Poisson's ratio. The shear modulus G is related to E and ν by $2G = \frac{E}{1+\nu}$. The readers are reminded that elastomers are almost incompressible, with $\nu = 1/2, E = 3G$.

Crack tip Fields:

Figure 1 shows a *traction free* planar crack with a straight front in a specimen. To study the local fields, we extend the crack front to infinity and consider a semi-infinite crack (hence avoiding considering the stress field near the edge E , see Appendix). We then carry out an asymptotic or local analysis by assuming that the displacement field near the crack front has the following form:

$$u_i = Ar^s f_i(\theta) , \quad r \rightarrow 0 \quad (4)$$

where (r, θ, z) is a cylindrical coordinate with z axis coinciding with the crack front. We require the stress fields derived from (4) to satisfy the traction free boundary condition on the crack faces. The idea is simple: substitute (4) into (1-3) and enforces the appropriate traction free boundary conditions. After some messy calculations, we discover that in general there are three independent solutions. They are of the form:

$$\bar{u} = \underbrace{\frac{K_I}{2G} \sqrt{\frac{r}{2\pi}} f'_\alpha(\theta) \bar{e}_\alpha}_{\bar{u}_I} + \underbrace{\frac{K_{II}}{2G} \sqrt{\frac{r}{2\pi}} f''_\alpha(\theta) \bar{e}_\alpha}_{\bar{u}_{II}} + \frac{2K_{III}}{G} \sqrt{\frac{r}{2\pi}} f'''(\theta) \bar{e}_3 \quad (5)$$

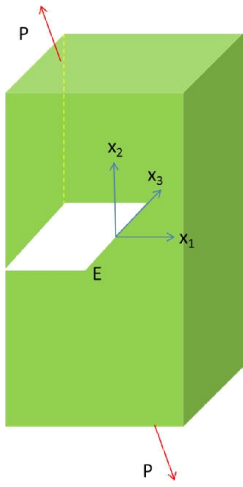


Figure 1: Geometry of a planar crack in a 3D specimen, the point E is the vertex where the crack front intersects the free surface (see discussion in Appendix regarding the local fields at E)

The three independent scalars K_I , K_{II} and K_{III} are called Mode I, II and III stress intensity factors respectively (units = $stress \times \sqrt{length}$). They cannot be determined by asymptotic or local analysis. Their values depend on the manner of loading and specimen geometry. For complicated geometries, their values will vary along the crack front, and they can only be determined by numerical methods. For simple geometries, they can be found in [1].

The functions $f'_\alpha(\theta)$, $f''_\alpha(\theta)$ and $f'''_3(\theta)$ are *universal* functions describing the angular variations of these local fields, they are found to be [2]:

$$\begin{cases} f'_1 \\ f'_2 \end{cases} = \begin{cases} \cos(\theta/2) [\kappa - 1 + 2 \sin^2(\theta/2)] \\ \sin(\theta/2) [\kappa + 1 - 2 \cos^2(\theta/2)] \end{cases} \quad \text{Mode I} \quad (6)$$

$$\begin{cases} f''_1 \\ f''_2 \end{cases} = \begin{cases} \sin(\theta/2) [\kappa + 1 + 2 \cos^2(\theta/2)] \\ -\cos(\theta/2) [\kappa - 1 - 2 \sin^2(\theta/2)] \end{cases} \quad \text{Mode II} \quad (7)$$

$$f''' = \sin(\theta / 2), \quad \text{Mode III} \quad (8)$$

where $\kappa = 3 - 4\nu$.

Here are some important points:

1. The displacement fields corresponding to Mode I is symmetric, that is,

$$u_1'(x_1, x_2) = u_1'(x_1, -x_2), u_2'(x_1, x_2) = -u_2'(x_1, -x_2) \quad (9)$$

In particular, on the crack faces $\theta = \pm\pi$, the crack opens symmetrically, the crack opening displacement (COD) is:

$$COD = u_2'(r, \theta = \pi) - u_2'(r, \theta = -\pi) = \frac{[\kappa + 1]}{G} K_I \sqrt{\frac{r}{2\pi}} \quad (10)$$

2. The displacement fields corresponding to Mode II is anti-symmetric, that is:

$$u_1''(x_1, x_2) = -u_1''(x_1, -x_2), u_2''(x_1, x_2) = u_2''(x_1, -x_2) \quad (11)$$

In Mode II, the crack does not open, the crack faces slide pass each other, and the relative slip on the crack face is

$$u_1'(r, \theta = \pi) - u_1'(r, \theta = -\pi) = \frac{[\kappa + 1]}{G} K_{II} \sqrt{\frac{r}{2\pi}} \quad (12)$$

Likewise, in Mode III, the crack faces slide pass each other in the out of plane direction, the relative slip is:

$$u_3'''(r, \theta = \pi) - u_3'''(r, \theta = -\pi) = \frac{4K_{III}}{G} \sqrt{\frac{r}{2\pi}} \quad (13)$$

Thus, local analysis shows that the displacement fields near the crack tip can be described by the superposition of three different modes of relative displacements of the crack faces.

3. The near tip displacements have the *universal* form given by (5-8), *irrespective of the specimen geometry and the manner of loading*. The displacement fields are directly proportional to the square root of the distance from the crack tip. Its magnitude is controlled by three scalar parameters - the stress intensity factors.

Since the stress fields are related linearly to the strains, and the strains are gradients of the displacements, the local stresses must be proportional to $1/\sqrt{r}$, that is, they become unbounded as the crack tip is approached. Using (6), (7) and (8), after some algebra, the *in-plane* stresses are given by [2]:

$$\begin{Bmatrix} \sigma_{11} \\ \sigma_{12} \\ \sigma_{22} \end{Bmatrix} = \frac{K_I}{(2\pi r)^{1/2}} \cos(\theta/2) \begin{Bmatrix} 1 - \sin(\theta/2) \sin(3\theta/2) \\ \sin(\theta/2) \cos(3\theta/2) \\ 1 + \sin(\theta/2) \sin(3\theta/2) \end{Bmatrix} \quad (14a)$$

$$\begin{Bmatrix} \sigma_{11} \\ \sigma_{12} \\ \sigma_{22} \end{Bmatrix} = \frac{K_{II}}{(2\pi r)^{1/2}} \begin{Bmatrix} -\sin(\theta/2) [2 + \cos(\theta/2) \cos(3\theta/2)] \\ \cos(\theta/2) [1 - \sin(\theta/2) \sin(3\theta/2)] \\ \sin(\theta/2) \cos(\theta/2) \cos(3\theta/2) \end{Bmatrix} \quad (14b,c)$$

$$\begin{Bmatrix} \sigma_{13} \\ \sigma_{23} \end{Bmatrix} = \frac{K_{III}}{(2\pi r)^{1/2}} \begin{Bmatrix} -\sin(\theta/2) \\ \cos(\theta/2) \end{Bmatrix}$$

It should be noted that the deformation and stress fields given in Mode I and Mode II above can be obtained by solving a *2 dimensional plane strain* crack problem, whereas the Mode III solution can be obtained by solving an *2 dimensional anti-plane* shear problem.

Recall, in plane strain deformation, the out of plane displacement u_3 is exactly zero; as a result,

$$\sigma_{31} = \sigma_{32} = 0 \quad \text{and} \quad \sigma_{33} = \nu(\sigma_{11} + \sigma_{22}) \quad (15)$$

Thus, directly ahead of the crack tip ($\theta=0$) of a Mode I crack, the near tip stress state is *hydrostatic* for an *incompressible* solid. Specifically,

$$\theta=0, \nu=1/2 \Rightarrow \sigma_{33} = \sigma_{11} = \sigma_{22} = \frac{K_I}{\sqrt{2\pi r}} \quad (16)$$

It is well known that plastic flow does not occur readily under hydrostatic stress, therefore, the plastic zone size (e.g. in metal) are usually quite small directly ahead of the crack tip. On the other hand, for elastomers, a hydrostatic stress state is known to favor nucleation of cavities.

The stress fields given by (14a,b) are also valid for plates subjected to in plane loading (no bending). These results can be obtained by plane stress analysis where the out of plane stress components σ_{3i} are assumed to be identically zero. Note that the in-plane stresses of a plane stress specimen (plate) is identical to that of a plane strain specimen - they are both given by (14a,b). The in-plane displacement fields are given by the first two terms of (5) provided that κ changes to $(3-\nu)/(1+\nu)$.

The elastic solution predicts that the stress and strain field is infinite as one approaches the crack tip. Since no material can support infinite stress (besides, linear elasticity assumes small strains, so the theory is no longer correct near the crack tip), the elastic solution cannot be valid all the way to the crack tip. The basis of LEFM is based on the *Small Scale Yielding* (SSY) assumption. Here is how Rice [3] describes it:

“The utility of elastic stress analyzes lies in the similarity of near crack tip stress distributions for all crack configurations. Presuming deviation from linearity to occur only over a region that is small compared to

geometrical dimensions (small-scale yielding), the elastic stress-intensity factor controls the local deformation field. This is the sense that two bodies with cracks of different size and with different manners of load applications, but which are otherwise identical, will have identical near tip deformation fields if the stress intensity factors are equal. Thus, the stress intensity factors uniquely characterizes the load sensed at the crack tip in situations of small-scale yielding, and criteria governing crack extension for a given local load rate, temperature, environment, sheet thickness (when plane stress fracture modes are possible), and history of prior deformation may be expressed in terms of stress intensity factors.....”

The story is more involved than what’s described above. For example, after substituting (4) into (1-3), you will discover three boundary value problems involving ordinary differential equations for the angular distribution functions f_α with s as an eigenvalue. In general, there are infinitely many eigenvalues (hence infinitely many eigenfunctions) that satisfies the traction free boundary conditions. The standard approach is to select the eigenvalue that give the *weakest* singularity (which turns out to be $-\frac{1}{2}$). The question is why we neglect these higher order singularities.

Since this idea is frequently passed over in fracture mechanics textbooks, I will illustrate it by considering Mode III. A detail description of this idea can be found in [3]. Since we are interested in local fields, we consider first the problem of a semi-infinite crack lying on the negative x_1 axis, with its tip at the origin. For anti-plane shear there is only one non-trivial displacement field, namely, $u_1 = u_2 = 0, u_3 = w(x_1, x_2)$. Using this assumption, one can show that all the in plane stress components and σ_{33} vanish with the exception of σ_{31} and σ_{32} which depend only on the in-plane coordinates. The governing equation is particularly simple, it is

$$\nabla^2 w = 0 \quad (17)$$

where ∇^2 is the two dimensional Laplacian operator. The traction free boundary condition for a Mode III crack reduces to

$$\sigma_{32}(r, \theta = \pm\pi) = 0 \Rightarrow w_{,2}(r, \theta = \pm\pi) = 0 \quad (18)$$

Substituting $w = r^s f(\theta)$ into (17) give rise to the following boundary value problem:

$$\frac{d^2 f}{d\theta^2} + s^2 f = 0 \quad \frac{df}{d\theta}(\theta = \pm\pi) = 0 \quad (19a,b)$$

The only anti-symmetric solution (since we physically expect that $w = 0$ for $\theta = 0$) that satisfy (19a) has the form:

$$f(\theta) = A \sin(s\theta) \quad (20)$$

where A is an arbitrary constant. For a non-trivial solution that satisfies the boundary condition (19b), we must have

$$\cos(s\pi) = 0 \quad (21)$$

This means that the eigenvalues are:

$$s = \frac{2n+1}{2} \quad \text{for any integer } n \quad (22)$$

The corresponding eigenfunctions are

$$f_n(\theta) = A_n \sin\left(\frac{2n+1}{2}\theta\right) \quad (23)$$

Note that the stress field given in (14c) corresponds to $s = \frac{1}{2}$ ($n = 0$). The stress fields corresponding to each eigenvalue can be obtained using the constitutive law $\sigma_{3\alpha} = Gw_{,\alpha}$. For convenience, we express the Cartesian stress components of $\sigma_{3\alpha} = Gw_{,\alpha}$ into their polar components. A simple calculation shows that

$$\begin{aligned} \tau_r &\equiv \sigma_{31} \cos\theta + \sigma_{32} \sin\theta = Gw_{,r} \\ \tau_\theta &\equiv \sigma_{32} \cos\theta - \sigma_{31} \sin\theta = G \frac{w_{,\theta}}{r} \end{aligned} \quad (24)$$

Thus, the near tip stress fields in polar coordinates are of the form:

$$\begin{pmatrix} \tau_r^n \\ \tau_\theta^n \end{pmatrix} = b_n r^{\frac{2n-1}{2}} \begin{pmatrix} \sin\left(\frac{2n+1}{2}\theta\right) \\ \cos\left(\frac{2n+1}{2}\theta\right) \end{pmatrix}, \quad b_n = \frac{2n+1}{2} GA_n \quad (25)$$

In a similar way, one can show that there are infinitely many eigenvalues and eigenfunctions for plane strain Mode I and II cracks (this is also true for interface cracks in elastic materials). Since each of these functions satisfies (17) and the traction free boundary condition, by linearity, any linear combination of them is also a solution near the crack tip. Therefore, one would expect the full expansion of the stress field near the crack tip should have the form:

$$\begin{pmatrix} \tau_r \\ \tau_\theta \end{pmatrix} = \begin{pmatrix} \sum_{n=-\infty}^{\infty} b_n r^{\frac{2n-1}{2}} \sin\left(\frac{2n+1}{2}\theta\right) \\ \sum_{n=-\infty}^{\infty} b_n r^{\frac{2n-1}{2}} \cos\left(\frac{2n+1}{2}\theta\right) \end{pmatrix} \quad (26)$$

Equation (28) shows that there are *infinitely many terms with higher singularity* than the $n = 0$ term.

The question is: why do we only select the $n = 0$ term (with an inverse square root singularity) despite the fact that there are infinitely many other terms that are more singular (and therefore

presumably more *dominant* as r approaches zero)? The standard arguments for keeping only the $n = 0$ term are:

- (i) The strain energy in the crack tip region must be bounded
- (ii) The displacement in the crack tip region must be bounded
- (iii) Uniqueness of elastic solution is lost if higher order solution are allowed
- (iv) The solution for the stress in the vicinity of an elliptic hole, in the limit of the aspect ratio goes to infinity, does not have such higher order singularities.

These are all flawed reasons. For example, (i) and (ii) above are violated by many solutions in linear elasticity that are used to represent physical phenomena. Examples include: a line load on the surface of a half space, a point load in a full space, and a dislocation in full space. All these solutions have unbounded energy and the first two have unbounded displacements. The displacement and energy singularities are not problematic in these solutions, because the solutions are not assumed to be applicable all the way to the singularity point. Rather, the solution is used only at distances that are large compared to the region over which the model (a load with no spatial extent and linear elastic behavior) is invalid. The same idea applies to fracture mechanics. Since no real material remains linear elastic when subjected to sufficiently large stresses, and no material can bear infinite stress or strains, there must be some region Ω surrounding the crack tip where the material behavior and changes in geometry deviate significantly from the prediction of linear elasticity. Inside Ω , which we called the process zone, the material behavior can be nonlinear, material surfaces may separate, voids and microcracks can nucleate and grow, continuum solution may not even be accurate etc.); outside this region, where linear elasticity is accurate, there is no singularity. Thus solutions that would have infinite displacement or energy if evaluated at the crack tip are not supposed to be used at the crack tip. In other words, the standard arguments about bounded displacement or strain energy do not legitimately rule out these higher order singular terms because these arguments make use of the linear elastic solution in a region where the solution is *a priori* known to be invalid.

The uniqueness assumption (iii) is also not justified. Since the strain energy is bounded outside the process zone Ω , the uniqueness condition (iii) is satisfied in the elastic region D which consists of material outside Ω , whether or not terms with higher order singularities are in the series description of the elastic field. Whether or not an entire fracture problem has a unique solution then depends on the material behavior inside the process zone. Uniqueness, if assumed to be valid for unknown material models in the process zone, is an additional postulate.

Finally, although one way of getting a flat or perfectly sharp crack is as the limit of an infinite aspect ratio elliptical hole (iv), a real crack is not necessarily well described by this limit. A mathematically sharp crack, if that is what one chooses to study, may be found as the limit of any number of non-singular fields. Many such limits lead to high order singularities in the limit of zero nonlinear zone size. For example, a cohesive zone model with both tensile and compressive stresses which goes appropriately to infinity as the cohesive zone size is reduced will lead to a traction free crack solution that does have high order singularities (see Lecture 2).

Having accepted at least the possibility of existence of these higher order singularities (which we shall demonstrate below), we need to reexamine the SSY condition where it is assumed that there is a region near the crack tip (but outside the process zone) where the K field dominates (despite the fact that there are infinitely many terms in the series that are more singular). *In fact, it is not sufficient that such a region exist, but that all specimens that satisfy SSY must share a common region surrounding the crack tip where K dominates.* Indeed, one naturally assumes that if the stresses are accurately known on the boundary of region that enclosed the crack tip, then the full (nonlinear material behavior, finite deformation etc.) stress and deformation fields inside the region can be determined by solving an appropriate boundary value problem. That is, one assumes that some kind of uniqueness assumption does hold for the crack tip material. To ensure the same local crack tip solution for two different specimens, the two crack tip regions associated with the specimens have to be effectively loaded by the same boundary conditions. Thus, any pair of bodies of identical material composition for which K is used to characterize fracture should have interior surface at the same distance from the crack tip where the stress field is dominated by the K field. To summarize, the SSY condition depends on the following conditions:

- the K field given by (14a,b,c) is dominant over all singular and non-singular terms in the series expansion (e.g. (26) for Mode III cracks), in some annular region surrounding the crack tip outside Ω .
- Specimens which are compared using SSY must have region of K dominance which has non-zero intersection. Thus, a radius r_k exists so that the K field dominates the stress field on all such specimens at r_k . This situation is illustrated for two specimens in Figure 2.

Some researchers have attempted to improve the accuracy of the stress field near the crack tip using a series expansion that ignored the existence of these higher order singular terms, e.g. in Mode I,

$$\sigma_{ij} = \frac{K_I}{\sqrt{2\pi}} r^{-1/2} \hat{\sigma}_{ij}^I(\theta, 0) + a_1 r^{1/2} \hat{\sigma}_{ij}^I(\theta, 1) + \dots + a_m r^{m-1/2} \hat{\sigma}_{ij}^I(\theta, m) + \dots \quad (27)$$

where $\hat{\sigma}_{ij}^I(\theta, m)$ are the eigenfunctions associated with the different eigenvalues describing the angular distribution of the stress fields. These eigenfunctions are universal functions independent of specimen geometry. However, if the higher order terms exist outside the process zone, any attempt to estimate or to calculate the a_m 's in (27) is not only futile but incorrect as infinitely many terms with $m < -1$ are thus neglected.

Let us again demonstrate this idea using a Mode III crack. Figure 3 shows a finite specimen loaded under antiplane shear condition. The crack tip is located at ($x_1=x=0, x_2=y=0$) and the process zone Ω is assumed to be sufficiently small so that it does not completely engulf the crack length. Let (r, θ) be a polar coordinate system attached to the crack tip. The term process zone means that inside this zone one or more of the usual assumptions regarding small strain linearity elasticity break down. Outside Ω linear elasticity is assumed to be exactly satisfied. The problem is shown in Fig. 3a, where C_1 and C_2 are circular boundaries enclosing the crack tip region. Between the circles, the material is purely linear

elastic. Thus we may consider the purely linear elastic problem in Figure 3b. The radius of C_1 , ρ is chosen to be as small as possible with Ω still being contained in C_1 ; that is, ρ is the outermost extent of Ω . The radius of C_2 is R , it is larger than ρ , and is chosen to be as large as possible while still contain in the specimen. The traction τ_r on these boundaries is assumed to be bounded so that

$$\begin{aligned} \tau_r(R, \theta) &= \tau_a F(\theta) && \text{(Outer boundary)} \\ \tau_r(\rho, \theta) &= \tau_0 H(\theta) && \text{(inner boundary)} \end{aligned} \quad (28a,b)$$

where τ_a and τ_0 are reference stresses defined by the maximum value of the tractions on the circles respectively. We shall assume that each of these prescribed tractions is separately self-equilibrated. Physically, one may think of τ_a as a scalar measure of the level of the applied load on the boundary of the specimen and τ_0 as a scalar measure of the inelastic stress at the outer boundary of the process zone Ω . For any actual specimen and confined process zone our replacement problem is exactly coincident with the solution to the original problem. Thus, the original singular and possibly nonlinear problem is reduced to the solution of a bounded linear problem.

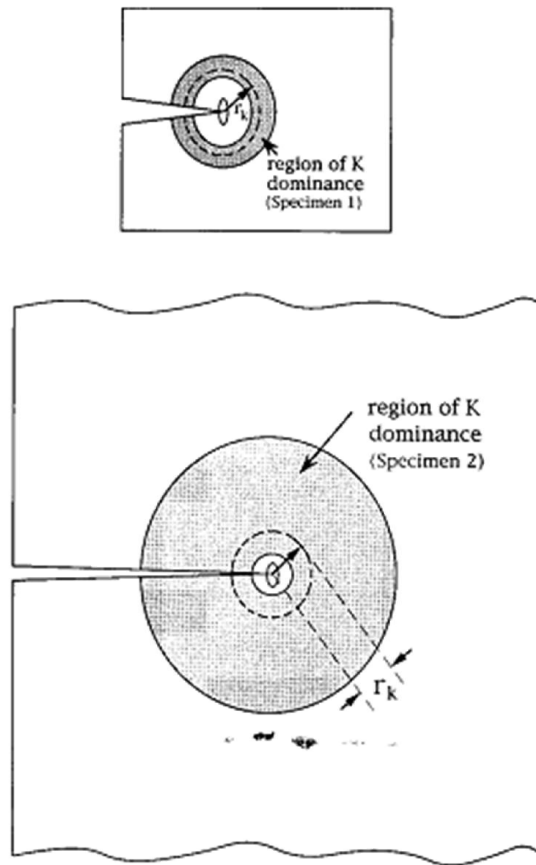


Figure 2: Two different specimens (I and II) made of the same material are shown. The region in which K field dominates is shaded in both cases. In order for the two specimens has the same fracture behavior, it is necessary that there exist a radius r_k that is the region of K dominance region for both specimen. The *same* elliptical region Ω at the crack tips represents a region where linear elasticity breaks down (they should be identical in shape and size if r_k exists).

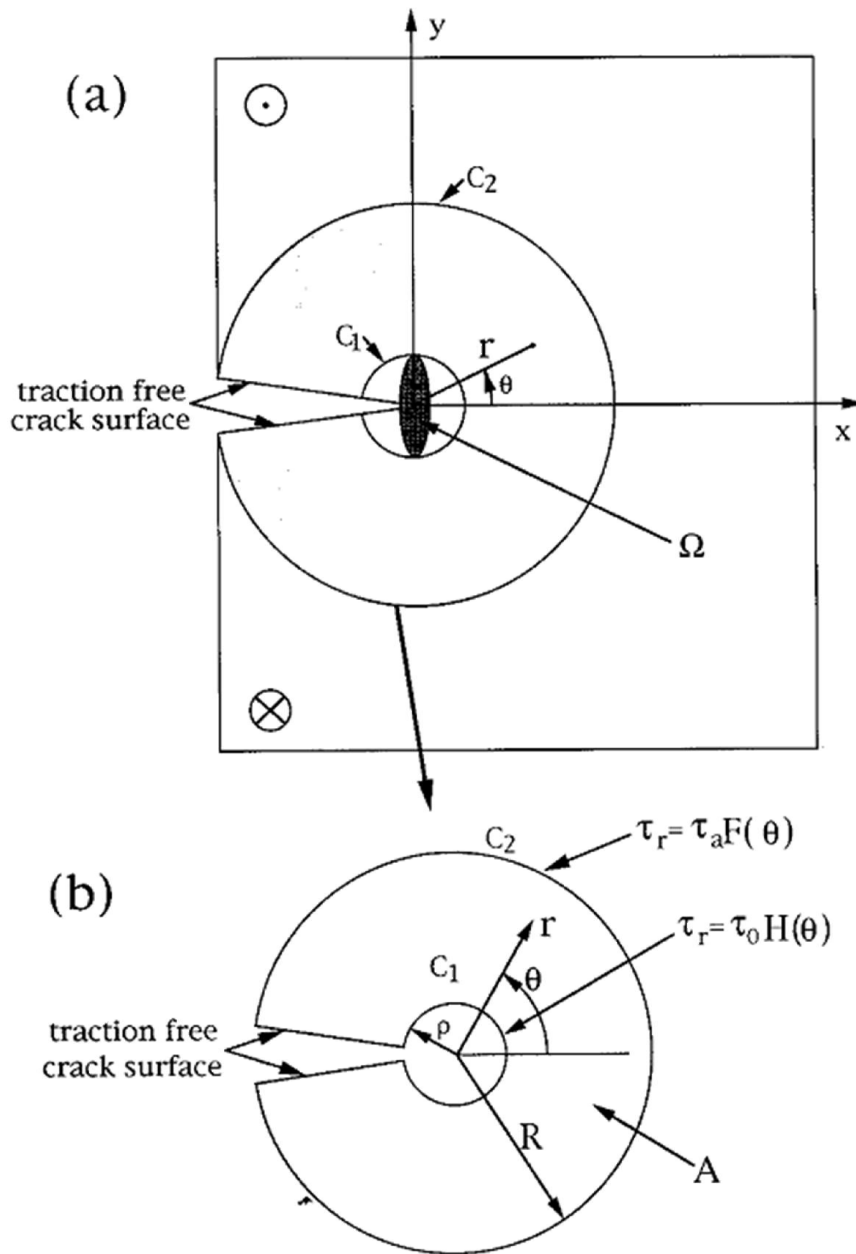


Figure 3a shows a specimen with two circles drawn. The inner circle is the small circle that can be drawn that completely encloses the nonlinear process zone, denoted by Ω . The material outside the inner circle C_1 (radius ρ) is homogeneous, isotropic and linearly elastic. The radius of the outer circle C_2

is R and is chosen so that $R > \rho$ and is as closed as possible to the specimen dimensions. (b) shows our replacement for the specimen in Fig. 3a. A specimen is considered in the region A that lies between the two circles. The tractions on these circular boundaries are the same as those occurring in the original specimen at the same locations.

Our approach is to first determine the stress field inside the region $A = \{\rho < r < R, -\pi < \theta < \pi\}$ in Figure 3b. This can be done by solving (17) subjected to boundary conditions (28a,b) and the traction free boundary condition

$$\tau_r(\rho < r < R, \theta = \pm\pi) = 0 \quad (28c)$$

on the crack faces. Closed form solution of (17) subjected to the boundary conditions (28a,b,c) is given as sum of two fields labelled I (inner surface traction free), O (outer surface traction free). Here I only state the result for the anti-symmetric case, which is of greatest interest to fracture. Details as well as the symmetric case can be found in [4].

$$\begin{pmatrix} \tau_r \\ \tau_\theta \end{pmatrix} = \tau_a \begin{pmatrix} \tau_r^I + \tau_r^O \\ \tau_\theta^I + \tau_\theta^O \end{pmatrix} \quad (29a)$$

$$\begin{aligned} \tau_r^I &= \sum_{n=0}^{\infty} b_n^I (r/R)^{(2n-1)/2} [1 - (\rho/r)^{2n+1}] \sin\left(\frac{(2n+1)\theta}{2}\right) \\ \tau_\theta^I &= \sum_{n=0}^{\infty} b_n^I (r/R)^{(2n-1)/2} [1 + (\rho/r)^{2n+1}] \cos\left(\frac{(2n+1)\theta}{2}\right) \\ \tau_r^O &= \frac{1}{\mu} \sum_{n=0}^{\infty} \varepsilon^{(2n+3)/2} b_n^{II} (r/R)^{(2n-1)/2} [1 - (R/r)^{2n+1}] \sin\left(\frac{(2n+1)\theta}{2}\right) \\ \tau_\theta^O &= \frac{1}{\mu} \sum_{n=0}^{\infty} \varepsilon^{(2n+3)/2} b_n^{II} (r/R)^{(2n-1)/2} [1 + (R/r)^{2n+1}] \cos\left(\frac{(2n+1)\theta}{2}\right) \end{aligned} \quad (29b-e)$$

where

$$\varepsilon \equiv \rho/R, \quad \mu \equiv \tau_a / \tau_0 \quad (29f)$$

and

$$\begin{aligned} b_n^I &= \frac{F_n}{1 - \varepsilon^{2n+1}}, & F_n &= \frac{1}{\pi} \int_{-\pi}^{\pi} F(\theta) \sin\left(\frac{2n+1}{2}\theta\right) d\theta, \\ b_n^{II} &= \frac{-H_n}{1 - \varepsilon^{2n+1}}, & H_n &= \frac{1}{\pi} \int_{-\pi}^{\pi} F(\theta) \sin\left(\frac{2n+1}{2}\theta\right) d\theta \end{aligned} \quad (29g,h)$$

Note that the functions τ_r^I, τ_r^O etc. are dimensionless. Also $\varepsilon \equiv \rho/R < 1$ and b_n^I, b_n^{II} are order one terms since both F and H are less than equal to 1. $(\tau_r^I, \tau_\theta^I)$ is the stress field if traction is applied on the

outer circle and no traction is applied on the inner circle whereas $(\tau_r^o, \tau_\theta^o)$ is the stress field if traction is applied on the inner circle and no traction is applied on the outer boundary. Note that the series solution is exact and consists of terms that are fractional powers of r and there is displacement discontinuity across the crack faces.

The results given by (29) above established that all the terms involving higher order singularities (i.e., second terms in square brackets in 29b-e) are present in the annular region A. Note that the coefficient of the $n = 0$ term in (29b-d) is related to the Mode III stress intensity factor K_{III} by

$$K_{III} = \left[\frac{1 - (H_0 / F_0) \varepsilon^{3/2} \mu^{-1}}{1 - \varepsilon} \right] \underbrace{\sqrt{2\pi R \tau_o F_0}}_{K_{III}^{applied}} \quad (30a)$$

where

$$K_{III}^{applied} = \sqrt{2\pi R \tau_o F_0} \quad (30b)$$

is the usual stress intensity factor, namely, the strength of the inverse square root singularity in specimen with a perfectly sharp structureless crack. Recall that (see (29g,h)) H_0, F_0 are order one terms and μ^{-1} is the ratio of the stress in the nonlinear zone to the applied traction on the outer boundary. Since we have not yet explicitly made any assumptions about material behavior in the process zone, quantities such as $\tau_o, \rho, \mu, \varepsilon$ are as yet unrelated.

If SSY is valid, the size of the process zone must be governed by K_{III} and τ_o . A dimensional argument requires that ρ must be proportional to K_{III}^2 / τ_o^2 . By (30a), K_{III} is approximately proportional $\tau_o \sqrt{R}$, we have

$$\varepsilon = C \mu^2 \quad (31)$$

where C is a positive dimensionless function of ε and is of order one. We can rewrite (30a) as

$$K_{III} = \left[\frac{1 - C\varepsilon}{1 - \varepsilon} \right] K_{III}^{applied} \quad (32)$$

where constants of order one were absorbed in C. As expected, only if the process zone is small in comparison with typical specimen dimensions, i.e., $\varepsilon = \rho / R \ll 1$ is the actual stress intensity factor K_{III} well approximated by the applied stress intensity factor $K_{III}^{applied}$.

Let us now examine the order of magnitude of each term in the series of in the annulus region A' defined by

$$A' = \{(r, \theta), r = \varepsilon^\lambda R, 1 > \lambda > 0\} \quad (33)$$

Note that A' is contain in A . The series solution can now be written in terms of $\varepsilon^\lambda R$. Let us first look at τ_θ^I (similar result applies to the other component)

$$\begin{aligned} \tau_\theta^I(r = \varepsilon^\lambda R) &= \sum_{n=0}^{\infty} b_n^I \varepsilon^{\lambda(2n-1)/2} [1 + \varepsilon^{(2n+1)(1-\lambda)}] \cos\left(\frac{(2n+1)\theta}{2}\right) \\ &= \sum_{n=0}^{\infty} b_n^I \varepsilon^{\lambda(2n-1)/2} \cos\left(\frac{(2n+1)\theta}{2}\right) + \sum_{n=0}^{\infty} b_n^I \varepsilon^{(2n-1)/2} [\varepsilon^{(1-\lambda)}]^{(2n+3)/2} \cos\left(\frac{(2n+1)\theta}{2}\right) \\ &= \dots + \underbrace{b_1^I \varepsilon^{\lambda/2}}_{r^{1/2}} \cos\left(\frac{3\theta}{2}\right) + \underbrace{b_0^I \varepsilon^{-\lambda/2}}_{r^{-1/2}} \cos\left(\frac{\theta}{2}\right) + \underbrace{b_0^I \varepsilon^{-\lambda/2+3(1-\lambda)/2}}_{r^{-3/2}} \cos\left(\frac{\theta}{2}\right) + \dots \end{aligned} \quad (34)$$

Examination of the terms in (34) reveals that the $r^{-1/2}$ has the smallest power in ε which is $\varepsilon^{-\lambda/2}$, thus in dominates over all other terms of the series (singular or non-singular) in A' in the limit as ε goes to zero.

Let us now apply the same procedure to τ_θ^O , the arrangement is:

$$\begin{aligned} \tau_\theta^O &= \frac{1}{\mu} \sum_{n=0}^{\infty} \varepsilon^{(2n+3)/2} b_n^{II} (\varepsilon^\lambda)^{(2n-1)/2} \cos\left(\frac{(2n+1)\theta}{2}\right) + \frac{1}{\mu} \sum_{n=0}^{\infty} \varepsilon^{(2n+3)/2} b_n^{II} (\varepsilon^{-\lambda})^{(2n-1)/2} \cos\left(\frac{(2n+1)\theta}{2}\right) \\ &= \frac{1}{\mu} \left[\dots + \underbrace{b_1^{II} \varepsilon^{5/2+\lambda/2}}_{r^{1/2}} \cos\left(\frac{3\theta}{2}\right) + \underbrace{b_0^{II} \varepsilon^{3/2-\lambda/2}}_{r^{-1/2}} \cos\left(\frac{\theta}{2}\right) + \underbrace{b_0^{II} \varepsilon^{3/2-3\lambda/2}}_{r^{-3/2}} \cos\left(\frac{\theta}{2}\right) + \dots \right] \end{aligned} \quad (35)$$

Note that in the second series (35), the $r^{-3/2}$ term is always the dominant term in A' as $\varepsilon \rightarrow 0$ which is $\mu^{-1} \varepsilon^{3/2-3\lambda/2}$. Since the stress is the sum of these two series, we must compare the dominate terms of both series, that is:

$$\varepsilon^{-\lambda/2} \text{ and } \mu^{-1} \varepsilon^{3/2-3\lambda/2} \quad (36)$$

Thus, the K field is dominant over all singular and non-singular terms if and only

$$\varepsilon^{-\lambda/2} \gg \mu^{-1} \varepsilon^{3/2-3\lambda/2} \Leftrightarrow \varepsilon^{-1+\lambda} \mu \varepsilon^{-1/2} \gg 1 \quad (37)$$

Recall (31) where $\mu^2 = C^{-1} \varepsilon$, substituting this expression into (37) and noting that C is a constant of order 1, the condition of K dominance reduces to

$$\varepsilon^{-1+\lambda} \gg 1 \quad (38)$$

which is always true for sufficiently small ε (the size of process zone small compare with specimen dimensions) since $\lambda < 1$. Thus, K dominance reduces to the usual statement of SSY (see Rice above).

We can now address the second issue that that specimens must have overlapping regions where the K field is dominant. This condition is satisfied since A' includes all λ in $(0,1)$ so long as (31) and (38) is satisfied. Of course, the smaller the ε , the more accurate is the K field and it is dominant over a larger region. In other words, the region of dominance for specimens with a larger value of $\varepsilon = \varepsilon_1$ is contained in the region of dominance of a specimen with a smaller value of $\varepsilon = \varepsilon_2$.

As a final example, we plot the shear stress $\tau_y(r, \theta = 0) = \tau_\theta(r, \theta = 0)$ directly ahead of the crack tip where the process zone Ω is a traction free hole (the material inside hole is a Jell-O) (see Figure 4 below). This solution is given by (29c). For this case, the local stress intensity factor increases by the amount $\varepsilon K_{III}^{Applied} / (1 - \varepsilon)$.

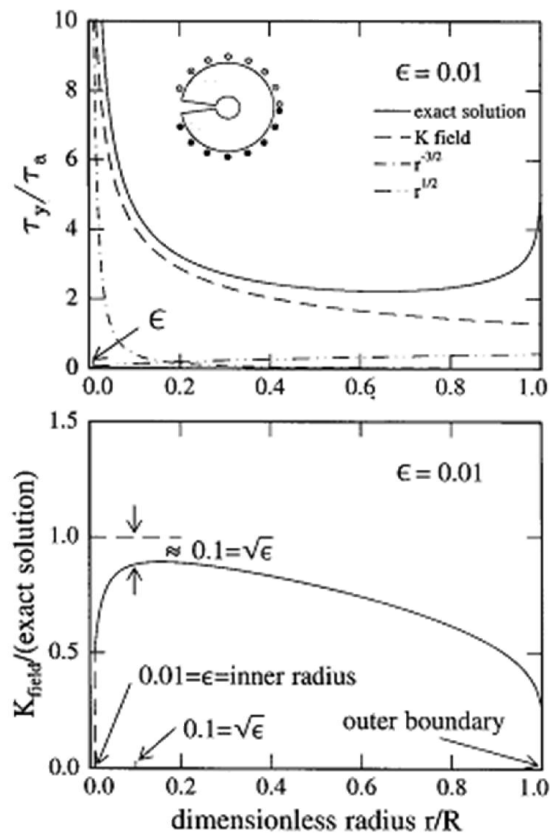


Figure 4a The shear stress τ_y directly ahead of the crack tip is plotted for the case of the traction free hole from $r/R = \varepsilon$ to $r/R = 1$ from the exact solution (29c) (solid line). The applied outer traction is a step function of θ . Also shown are the K field, i.e., the $r^{-1/2}$ term (dash line), the $r^{-3/2}$ term (dotted line) and the $r^{1/2}$ term (dot dot dash) in the series expansion. Note that the $r^{-3/2}$ term is actually larger than the $r^{1/2}$ term for $r/R < 0.2$. Figure 4b plots the ratio of the K field to the exact solution. This figure shows that the solution for this particular problem is consistent with the general result that the K field is most accurate at $r \approx \sqrt{\varepsilon}R$ where the fractional error of the K field compare to the exact solution is of order $\sqrt{\varepsilon}$.

Criterion on fracture initiation:

Assuming SSY holds, then the criterion for fracture initiation in Mode I (for sufficiently thick specimens) is

$$K_I = K_{IC} \quad (39)$$

It is important to note that K_{IC} is a material property (sometimes called fracture toughness) that cannot be determined from elasticity analysis. It is determined by testing. The left hand side of the equation is a quantity that is determined by carrying out an elastic calculation accounting for the specimen geometry and the applied load. In a perfectly brittle material when K reaches K_{IC} the crack grows unstable in a load controlled test. However, ductile materials can resist crack growth and requires $K > K_{IC}$ to continue crack growth.

The utility of the SSY concept is important for practical applications such as correlating crack growth rate data in fatigue crack growth and slow growth of cracks under high temperature conditions (creep crack growth). In fatigue crack growth, the applied cyclic loads are typically very small so for sufficiently long cracks, SSY is satisfied¹. The material behavior in the nonlinear process zone is very complicated (due to repeating loading and unloading, formation of slip bands etc.). However, SSY allows us to conclude that the crack growth rate must be controlled by the elastic K field; therefore, it is the correct parameter to correlate data.

References:

- [1] The stress analysis of cracks handbook, 3rd edition: by Hiroshi Tada, Paul C. Paris and George R. Irwin. ASME press.
- [2] J.R. Rice, in Fracture, H. Liebowitz (ed.), vol.2 Academic Press, NY (1968), p191.
- [3] C.Y. Hui and A. Ruina, Intl. J. Fracture, 72: 97-120, 1995
- [4] John W. Hutchinson, "A course on Nonlinear Fracture Mechanics", Department of Solid Mechanics, The Technical University of Denmark, 1979.

¹ Most of the life time of fatigue cracks in real structures can be spend in the regime where the crack is very small, in this regime, SSY is likely to be violated.

Appendix:

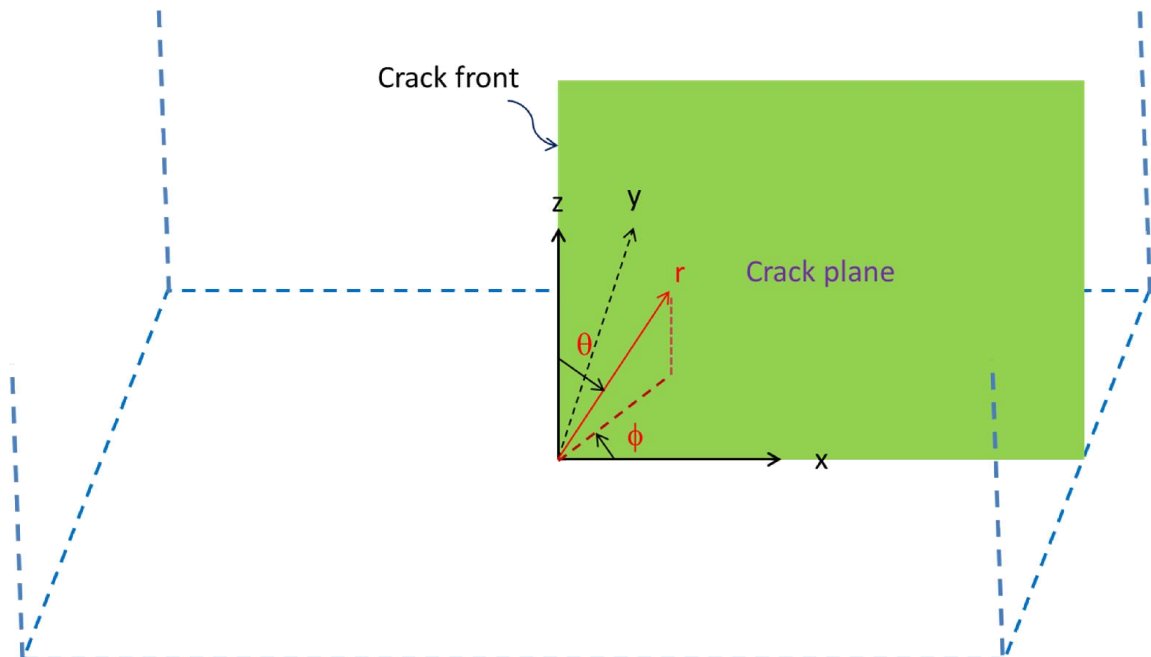
The stress near the edge is complicated and was studied first by J. P. Benthem, "State of stress at the vertex of a quarter-infinite crack in a half space", Int. J. of solids & Structures, 1977. Vol. 13. pp. 479. By limiting his analysis to stresses that are symmetrical to the crack plane, he showed that the stress field at the vertex of a quarter-infinite crack in a half space ($z > 0$), see picture below, has the form given by

$$\sigma_{ij} = Ar^\lambda f_{ij}(\theta, \phi)$$

where (r, ϕ, θ) is a spherical coordinate system with origin at the vertex where the crack intersects the surface of the half space (note that (r, θ) is defined differently in here than in the main text of this lecture). In figure above, the crack occupies the half plane $z > 0$, $x > 0$ and $y = 0$ with its front along the positive z axis. The order of singularity, λ depends on the Poisson's ratio, for the special case of $\nu = 0$, $\lambda = -1/2$ (note $\sigma_{33} = 0$ in this case, see (15)). In general, λ increases with Poisson's ratio, and equals to -0.3318 for the case of an incompressible solid. Thus, the corner singularity is weaker than the square root singularity of the crack tip solution. It can be shown that if one approaches the crack front $z > 0$ from $x < 0$, $y = 0$,

$$\sigma_{yy}(-x \rightarrow 0^+, y = 0, z) \propto \frac{z^{\lambda+1/2}}{\sqrt{|x|}}$$

Since $\lambda < 1/2$ except for Poisson's ratio = 0, the stress intensity factor vanishes as one approaches the crack front from the corner.



Lecture 2: Energy release rate and Introduction to cohesive zone model

There are several ways to derive the energy release rate of a crack in a *perfectly linear elastic solid* with a *structureless* crack tip (higher order singular terms are not present). A favorite version of mine was due to John Hutchinson in his notes on Nonlinear Fracture Mechanics (see Reference [4] in lecture 1) which is reproduced below with some minor modifications. Consider a plane strain or plane stress elastic sample loaded in Mode I with an initial straight crack of length a subjected to displacement boundary conditions (later we will see that the energy release rate is independent of the nature of the loading system, so we could have applied traction boundary conditions, for example). Consider a straight advance of the crack tip resulting in the crack length increasing from a to $a + \Delta a$, during this advance the displacements prescribed on the specimen boundaries remains fixed. Thus, the potential energy of the system is the strain energy of the specimen. We compute this change in strain energy by observing that before the crack is advanced the traction acting the crack plane ($y = 0$) is $\sigma_{22}(x, 0)$ and for very small Δa , it is given by

$$\sigma_{22}(x, 0) = \frac{K_I(a)}{\sqrt{2\pi x}} \quad 0 < x \leq \Delta a \quad (2.1)$$

where x is the distance directly ahead of the crack tip, see picture below (copied from Hutchinson's book). In (2.1), $K_I(a)$ denotes the Mode I stress intensity factor under the prescribed displacement at crack length a .

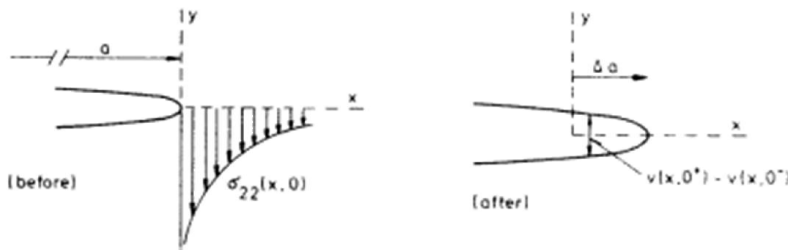


Figure 1

The energy release during the extension, $\Gamma \Delta a$ ¹, is the negative of the work done by the traction $\sigma_{22}(x, 0)$ and this is (due to linear elasticity):

$$\Gamma \Delta a = \frac{1}{2} \int_0^{\Delta a} \sigma_{22}(x, 0) [v(x, 0^+) - v(x, 0^-)] dx \quad (2.2)$$

where $v(x, 0^+) - v(x, 0^-)$ is the separation of the crack faces in the *final* position when the crack is at $a + \Delta a$. Since Δa is very small, we can compute this separation using the asymptotic result (eq. 10 in lecture 1), that is,

¹ The standard notation for the energy release rate is G , which I used to denote the shear modulus.

$$v(x,0^+) - v(x,0^-) = \frac{[\kappa+1]}{G} K_I(a+\Delta a) \sqrt{\frac{\Delta a-x}{2\pi}} \quad (2.3)$$

Substituting (2.1 & 2.3) into (2.2) gives:

$$\Gamma \Delta a = \frac{1}{4\pi} \frac{[\kappa+1]}{G} K_I(a) K_I(a+\Delta a) \int_0^{\Delta a} \sqrt{\frac{\Delta a-x}{x}} dx = \frac{\kappa+1}{8G} K_I(a) K_I(a+\Delta a) \Delta a \quad (2.4)$$

Taking the limit as Δa goes to zero gives the energy release rate Γ (unit = energy/area), i.e.

$$\Gamma = \frac{\kappa+1}{8G} K_I^2 \quad (2.5)$$

For plane strain, $\kappa = 3 - 4\nu$. For plane stress, $\kappa = \frac{3-\nu}{1+\nu}$. Thus,

$$\begin{aligned} \Gamma &= \frac{1-\nu^2}{E} K_I^2 && \text{(plane strain)} \\ \Gamma &= K_I^2 / E && \text{(plane stress)} \end{aligned} \quad (2.6a,b)$$

The argument above can be repeated for Mode II and Mode III cracks. Since the modes are decoupled, the energy release Γ per unit crack advance is

$$\Gamma = \frac{1-\nu^2}{E} (K_I^2 + K_{II}^2) + \frac{1}{2G} K_{III}^2. \quad (2.7)$$

In the derivation above, the specimen is under displacement controlled so that the potential energy change of the system is the change in strain energy of the specimen. We now showed that the energy release rate is independent of the nature of the loading system. The derivation below is due to Hutchinson [4]. Consider a crack body loaded in Mode I by a testing machine with compliance C_M (represented by a spring with stiffness $1/C_M$ in Figure 2 below). Note C_M is independent of crack length.

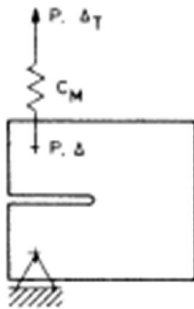


Figure 2

Let Δ_T denote the total displacement which will be regarded as prescribed. The total energy of the system (machine + sample) is the strain energy of the spring + the strain energy of the sample. The load P acting on the spring (as well as the sample) is

$$P = \frac{\Delta_T - \Delta}{C_M} \quad (2.8)$$

where Δ is the displacement of sample at the load point. Thus, the strain energy of the spring is

$$\frac{(\Delta_T - \Delta)^2}{2C_M} \quad (2.9)$$

The strain energy of the sample is given by

$$\frac{P}{2} \Delta = \frac{\Delta^2}{2C(a)}, \quad (2.10)$$

where $C(a) = \Delta / P$ is the compliance of the sample (which is assumed to be linearly elasticity) and depends on the crack length a (for a given sample, the compliance increases with crack length). The total potential energy of the system, PE, is the sum of the strain energies of the sample and the spring, that is,

$$PE = \frac{(\Delta_T - \Delta)^2}{2C_M} + \frac{\Delta^2}{2C(a)} \quad (2.11)$$

The energy release rate Γ is the change in potential energy of the system per unit area of crack extension at fixed prescribed displacement Δ_T ,

$$\Gamma b = \left. \frac{\partial PE}{\partial a} \right|_{\Delta_T} = \underbrace{\frac{-(\Delta_T - \Delta)}{C_M}}_{-P} \frac{d\Delta}{da} + \underbrace{\frac{\Delta}{C(a)}}_P \frac{d\Delta}{da} + \frac{1}{2} \frac{\Delta^2}{C^2(a)} \frac{dC}{da} = \frac{P^2}{2} \frac{dC}{da} \quad (2.12)$$

where b is the thickness of the specimen. The final result is independent of the machine compliance. Note that an infinitely stiff machine ($C_M \rightarrow \infty$) corresponds to a displacement controlled test, whereas an infinitely soft machine ($C_M \rightarrow 0$) corresponds to a force controlled test. In addition, eq.(2.12) allows us to determine the energy release rate in a specimen by measuring the change in compliance of two specimens with slightly different crack lengths.

Example 1

Consider the cantilever beam specimen shown in Figure 3 below. The compliance of the specimen $C(a)$ can be estimated using beam theory, it is:

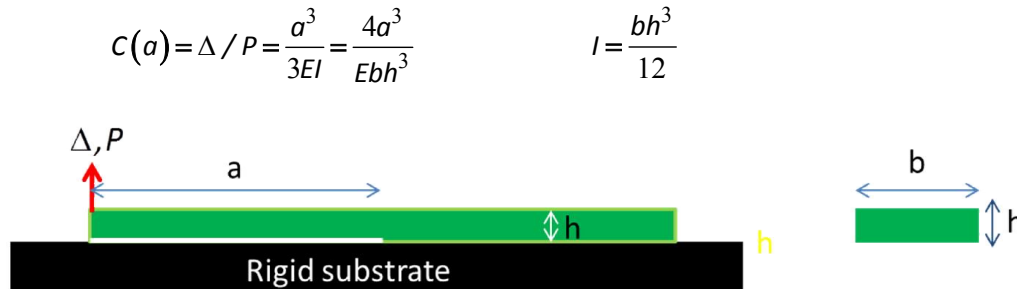


Figure 3 Side-view of a cantilever beam specimen, a is the crack length. The beam has a rectangular cross-section with width b and height h . The specimen is assumed to be perfectly bonded to a rigid substrate. Caution: the loading is not pure mode I (why?)

The energy release rate under displacement control is obtained from 2.12,

$$\Gamma = \frac{\Delta^2}{2bC^2(a)} \frac{dC}{da} = \frac{3Eh^3}{8} \frac{\Delta^2}{a^4}$$

Note that in a displacement controlled test, the energy release rate decreases with crack length, hence crack growth is generally stable under displacement controlled. You can show easily that in a load controlled test, $\Gamma = \frac{6a^2 P^2}{Eh^3 b^2}$, so energy release rate increases with crack length.

Here are some points:

1. (2.7), when specialized to a Mode I crack, shows that the energy release rate (a global quantity) is directly related to the local quantity K_I which characterize the strength of the crack tip fields. In particular, it shows exactly how the stress intensity factor is related to the change in compliance of the structure due to crack growth.
2. The Griffith fracture criterion, which is based on energy balance is equivalent to the stress intensity factor based fracture criterion. For a Mode I crack,

$$K_I = K_{IC} \Leftrightarrow \Gamma = G_{IC} \Leftrightarrow G_{IC} = K_{IC}^2 / E^* \quad (2.13)$$

3. The above derivation assumes that the material is perfectly elastic all the way to the crack tip and that the inverse square root singular field is the only singular term. Therefore, only a perfectly elastic solid with a structureless crack tip is the energy release rate given by (2.7).

A different way of deriving the energy release rate (J integral)

A derivation of energy release rate that does not require a purely elastic solid and introduces the concept of translation invariance which naturally leads to the well-known path independent J integral is given here. In the derivation below, I assume the material is elastic everywhere, except for a small region Ω surrounding the crack tip. In this region, the material need not be elastic, in fact the

local fields may not be continuous (e.g. the material may separate directly ahead of Mode I crack, see cohesive zone model below). However, I still assume mechanical energy is a well-defined quantity.

The crack is assumed to be planar with a straight front. In addition, the stress and deformation fields are independent of the out of the plane direction (e.g. the sample can be loaded in plane strain, in plane stress or in anti-plane shear). The crack is assumed to grow in the positive X direction with speed $\dot{a}(t)$ ², as shown in Fig.4a below. Let (X, Y) be a fixed coordinate system in the laboratory specifying the coordinates of a material point. Let (x_1, x_2) be a coordinate system attached to the tip of the moving crack.

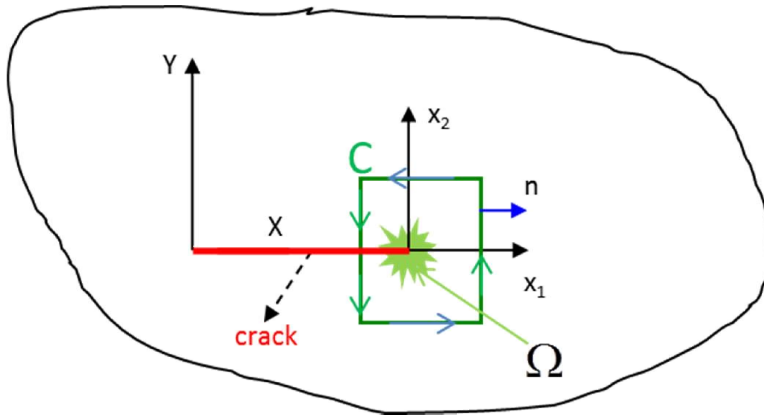


Figure 4a (X, Y) is a fixed or Lab. frame whereas (x_1, x_2) is a frame attached to the crack tip which is moving at $\dot{a}(t)$. The process zone $\Omega(t)$ is contained inside the contour C, which translates with the moving crack tip.

Let C be a fixed continuous curve that starts from a point on the lower crack face, goes around the crack tip in anti-clockwise direction, and ends at a point (not necessary the same point) on the upper crack face. We select C to be the smallest curve so that it completely encloses $\Omega(t)$ and such that the material outside and on C is elastic (see Fig. 4a, the curve in Fig. 4a is a rectangle, but you can use a circle or some other appropriate smooth curve). We denote the area inside C by A ($A - \Omega$ can be viewed as a transition zone where material changes behavior). Thus, stresses and deformations are continuous across C. With respect to the moving frame (x_1, x_2) , C is *fixed*. That is, C can be described by

$$x_1 = f(s), x_2 = g(s) \quad (2.14)$$

where s is the arc length. Note that A is a region of ever changing material points. Note also that $x_2 = Y$ and

² \dot{a} is much slower than wave speed so the crack moves in a quasi-static fashion.

$$x_1 = X - \int_0^t \dot{a}(\tau) d\tau \quad (2.15)$$

The amount of energy flow to the crack tip *per unit time*, defined as $\Gamma \dot{a}$, is the rate of traction work acting on material particles that coincides instantaneously with the curve C minus the rate of change of mechanical energy of material points Λ_C inside C, and is denoted by $\dot{\Lambda}_C$. The rate of stress work acting on material particles that lies on C is:

$$\int_C \sigma_{ij}(x_1(s), x_2(s), t) n_j(x_1(s), x_2(s)) \dot{u}_i(x_1(s), x_2(s), t) ds \quad (2.16a)$$

Here

$$\sigma_{ij}(x_1, x_2, t) = \sigma_{ij}(X - \int_0^t \dot{a}(\tau) d\tau, Y, t) \equiv \Sigma_{ij}(X, Y, t) \quad (2.16a)$$

$$u_i(x_1, x_2, t) = u_i\left(X - \int_0^t \dot{a}(\tau) d\tau, y, t\right) \equiv U_i(X, Y, t) \quad (2.16b)$$

where U_i are the displacements of the material point at (X, Y) and s is the arc length on C. *Note that the unit outward normal vector \vec{n} of C as well as the curve itself does not depend on t since the integration is performed in the moving frame.* In (2.16a), $\dot{u}_i(x_1(s), x_2(s), t)$ is the material derivative of the material point at (X, Y) , that is,

$$\left. \frac{\partial U_i(X, Y, t)}{\partial t} \right|_{X, Y} \equiv \dot{u}_i(x_1, x_2, t) = -\dot{a}(t) \left. \frac{\partial u_i(x_1, x_2, t)}{\partial x_1} \right|_{t, x_2} + \left. \frac{\partial u_i(x_1, x_2, t)}{\partial t} \right|_{x_1, x_2} \quad (2.17)$$

Combining (2.17) and (2.16a), the rate of stress work acting on material particles that coincides instantaneously with the curve Γ is:

$$\int_C \sigma_{ij} n_j \left[-\dot{a} \frac{\partial u_i}{\partial x_1} + \frac{\partial u_i}{\partial t} \right] ds \quad (2.18)$$

where all relevant quantities are written using coordinates in the moving frame of reference and for the sake of keeping the notation simple, I have not included the independent variables in the arguments of the functions in (2.18).

Next, we find $\dot{\Lambda}$ on material points that lies inside C. Note we have to compute the change of mechanical energy on the same material points. The material points inside C are changing with time in the material frame (Lab. frame). Therefore, we use Reynolds's transport theorem and found

$$\dot{\Lambda} = \frac{\partial \bar{w}_A}{\partial t} - \dot{a}(t) \int_C w(x_1, x_2, t) n_{x_1} ds \quad (2.19)$$

Here $\partial \bar{w}_A / \partial t$ is the rate of change of mechanical energy inside A with respect to the moving frame. Note that if the local fields are continuous everywhere (e.g. inside $\Omega(t)$), then we can write the first term in (2.19) as

$$\int_A \left. \frac{\partial w(x_1, x_2, t)}{\partial t} \right|_{x_1, x_2} dx_1 dx_2$$

where w in the above equation is the amount of stress work on a material point which is at (x_1, x_2) . Specifically, the stress work on a material particle at (X, Y) is defined by:

$$w(X, Y, t) = \int_{\gamma} \Sigma_{ij}(X, Y, t') dE_{ij}(X, Y, t') \quad (2.20)$$

where E_{ij}, Σ_{ij} is the infinitesimal strain and stress tensor expressed in material frame (X, Y) , and γ is a curve or path in the strain space from $E_{ij} = \mathbf{0}$ to $E_{ij}(X, Y, t)$: that is, γ denote the strain history of the material point occupying (X, Y) from $t = 0$ to the current time t . Note that w defined in (2.16) does not assume the existence of a strain energy density function and is valid for any stable materials.

A simple way to understand (2.19) is as follows: the first term on the RHS of (2.19) is the rate of change of the total mechanical energy relative to the moving frame. The problem with this term is that we are interested in the rate of stress work on the material points inside C at time t (that is, we are following this set of material points). However, as the moving frame (crack tip) moves from t to $t + dt$, material points inside C close to its left edge *exit* this edge whereas material points just outside the right edge of C *enters* C through this edge (it is easy to visualize this if the curve C is a rectangle, such as the one shown above). Since our goal is to compute the rate of stress work on the same set of material points which was inside C at time t , we must add the energy of those material points that exit the left edge of C and subtract the energy of those material points that enter the right edge from the first term $\frac{\partial \bar{w}_A}{\partial t}$ in (2.19). Mathematically, this means subtracting $\dot{a}(t) \int_C w(x_1, x_2, t) n_{x_1} ds$ from the 1st term in (2.19).

The energy flow to the crack tip per unit time, $\Gamma \dot{a}$ is obtained by subtracting (2.19) from (2.18),

$$\begin{aligned}
\Gamma \dot{a} &= \int_C \sigma_{ij} n_j \left[-\dot{a} \frac{\partial u_i}{\partial x_1} + \frac{\partial u_i}{\partial t} \right] ds - \left[\frac{\partial \bar{w}_A}{\partial t} - \dot{a}(t) \int_C w(x_1, x_2, t) n_{x_1} ds \right] \\
&= \dot{a} \int_C \left(w(x_1, x_2, t) n_{x_1} - \sigma_{ij} n_j \frac{\partial u_i}{\partial x_1} \right) ds + \left[\int_C \sigma_{ij} n_j \frac{\partial u_i}{\partial t} \Big|_{x_1, x_2} ds - \frac{\partial \bar{w}_A}{\partial t} \right] \quad (2.21)
\end{aligned}$$

In general, the term inside the square bracket in (2.21) is not zero. It is zero when we have steady state inside the C, that is, the fields inside C are *independent* of time. Note that, for steady state condition to exist, the material must be *homogeneous* in the x direction and the crack speed independent of time, i.e., $\dot{a}(t) = \dot{a}_{ss}$. Also, $\Omega(t) = \Omega_{ss}$ is independent of time. Thus, for steady state, the energy flow to the crack tip per unit time is given by

$$J_c \dot{a}_{ss} = \left[\int_C \left(w(x_1, x_2, t) n_{x_1} - \sigma_{ij} n_j \frac{\partial u_i}{\partial x_1} \right) ds \right] \dot{a}_{ss} \quad (2.22)$$

Since the material is elastic outside and on C, J_c is independent of path. Specifically, the same value of the path integral is obtained for all paths γ enclosing the crack tip (in the manner described above) as long as these paths lies outside C (see Fig.4b). To prove this, we note that for any close path C' that lies inside an elastic region that contains no singularities, the J integral, defined by

$$J \equiv \int_{C'} \left(w n_1 - \sigma_{ij} n_j \frac{\partial u_i}{\partial x_1} \right) ds \quad (2.23)$$

is zero. This is because

$$\begin{aligned}
\int_{C'} w n_1 ds &= \int_{A'} w_{,1} dx_1 dx_2 = \int_{A'} \underbrace{\frac{\partial W}{\partial \varepsilon_{ij}}}_{\sigma_{ij}} \frac{\partial \varepsilon_{ij}}{\partial x_1} dx_1 dx_2 = \frac{1}{2} \int_{A'} \sigma_{ij} \left(\frac{\partial u_{i,j}}{\partial x_1} + \frac{\partial u_{j,i}}{\partial x_1} \right) dx_1 dx_2 = \\
&= \int_{A'} \sigma_{ij} u_{i,j,1} dx_1 dx_2 = \int_{A'} \left[\left(\sigma_{ij} u_{i,1} \right)_{,j} - \underbrace{\sigma_{ij,j}}_0 u_{i,1} \right] dx_1 dx_2 = \int_{C'} \sigma_{ij} n_j \frac{\partial u_i}{\partial x_1} ds
\end{aligned} \quad (2.24)$$

Let us use this result to show that paths such as γ in Figure 4b satisfy

$$J_\gamma = \int_\gamma \left(w n_1 - \sigma_{ij} n_j \frac{\partial u_i}{\partial x_1} \right) ds = \int_C \left(w n_1 - \sigma_{ij} n_j \frac{\partial u_i}{\partial x_1} \right) ds = J_C \quad (2.25)$$

To see this, construct the close path $C' = -\gamma + C + \omega_1 + \omega_2$ in Figure 4b. Clearly, C' does not enclose any singularities, so J integral on C' is zero. Note the integrand of J on ω^+, ω^- is identically zero (since $n_1 = 0$ and crack surfaces are traction free), using $J_\gamma = -J_{-\gamma}$ proves (2.25).

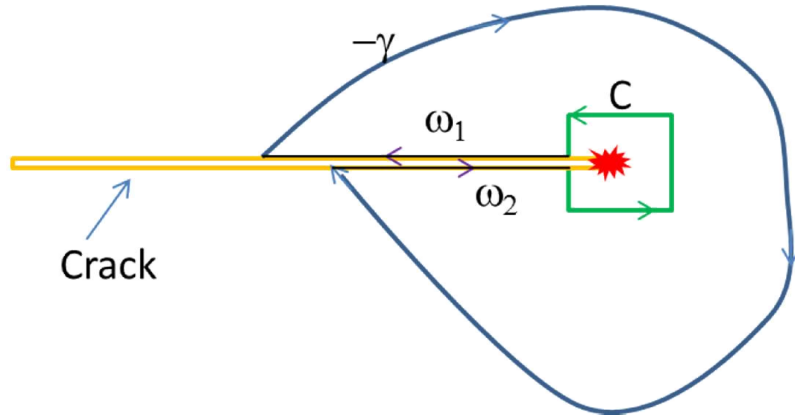


Figure 4b Diagram showing the definition of the curves $\gamma, -C, \omega_1$ and ω_2 .

For a perfectly linear elastic solid with a structureless crack tip, the energy release rate can be computed using the elastic near tip fields in the first lecture by shrinking the contour C all the way to the crack tip. For example, take C to be a circular contour of radius $\delta \rightarrow 0$ with center at the crack tip. The calculations are slightly messy, but you may be interested in noting that since the stress and strain field behaves like $r^{-1/2}$ near the crack tip, terms in the J integral behaves like $1/\delta$ on the circular path and $ds = \delta d\theta$, so δ cancels out and you have an integral in θ only. After some calculation, you will recover (2.7) with $J = \Gamma$.

It is important to note that (2.7) assumes that the material is linearly elastic all the way to the crack tip, which cannot be possibly true in practical situations. In general, if there are nonlinear effects, then

$$J \neq \frac{1-\nu^2}{E} (K_I^2 + K_{II}^2) + \frac{1}{2G} K_{III}^2 \quad (2.26)$$

To see this, let us return to the anti-plane shear problem in lecture 1. Note that the actual K field at the crack tip is modified by the presence of the nonlinear zone, so one possibility is $J = \frac{1}{2G} K_{III}^2$, where K_{III} is the modified stress intensity factor due to the existence of the process zone. This is *incorrect*. We can check by using the exact solution (given by eq. (29) in lecture 1) to evaluate the J integral for any path (a circular one for convenience) inside the annulus region. *Note that if we neglected all the higher order singularity terms in the series and keeping only the non-singular terms + the K field, we will find*

$$J = \frac{1}{2G} (K_{III}^{Applied})^2 \quad (2.27)$$

This is because the remaining non-singular terms cannot contribute to the J integral since these terms and their products with any other terms in the series (including the K term) are bounded as r goes to zero. Using the path independence of J and shrinking the radius of the integration path to zero gives 2.27). On the other hand, if the entire series is used, terms like $r^{-3/2}$ and $r^{1/2}$ can cross multiply giving rise to terms with $1/r$ which leads to non-trivial contributions to J. If you carried out the calculation using these series, you should find:

$$J = \frac{\pi R \tau_a^2}{G} d_0^2 + 2 \sum_{n=0}^{\infty} d_{n+1} e_n \quad d_n = b_n' + \varepsilon^{(2n+3)/2} \mu^{-1} b_n'', \quad e_n = b_n' \varepsilon^{(2n+1)} + \varepsilon^{(2n+3)/2} \mu^{-1} b_n'' \quad (2.28)$$

where

$$\begin{aligned} b_n' &= \frac{F_n}{1 - \varepsilon^{2n+1}}, & F_n &= \frac{1}{\pi} \int_{-\pi}^{\pi} F(\theta) \sin\left(\frac{2n+1}{2}\theta\right) d\theta, \\ b_n'' &= \frac{-H_n}{1 - \varepsilon^{2n+1}}, & H_n &= \frac{1}{\pi} \int_{-\pi}^{\pi} F(\theta) \cos\left(\frac{2n+1}{2}\theta\right) d\theta \end{aligned} \quad (2.29)$$

Recall that the pure elastic K_{III} is $K_{III}^{Applied} = \pi \tau_a F_o \sqrt{R}$, thus the J integral only equals $J = \frac{1}{2G} (K_{III}^{Applied})^2$ if and only if $\varepsilon = 0$ (there is no non-linear zone). Equation (2.30a) shows that there are two contribution to the J integral due to the existence of the non-linear zone, the first one is due to the change in stress intensity factor which is order ε , the second one is of the same order in ε and is due to the interaction of the higher order singular terms and the non-singular terms.

The discussions above introduce an important concept in mechanics: *configuration force*. That is, we can think of the J integral as a force (force/per unit length) due to a change in position of the crack (a simple example of a configuration force is the action of gravity on a mass). A beautiful example of energy release rate as a configuration force is a 90° peel test (see Fig. 4c below) where the peel arm consisting of a *stiff* sheet (so we can neglect the deformation of the sheet at the place where the load F is applied), see Figure 4c below. The energy release rate is equal to the peel force per unit width.

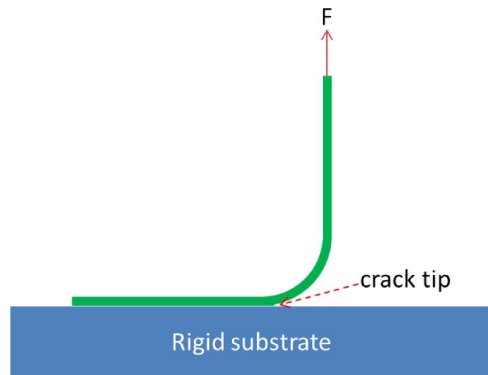


Figure 4c Schematic of a 90° peel test: A thin elastic sheet of width w (not shown, in out of plane direction) is glued to the surface of a flat rigid substrate and peel at a steady rate v in the direction

perpendicular to the substrate. The peel force F is actually the total load applied to the sheet divided by w , so it has units of energy/area (the same as energy release rate).

Examples using J integral to compute energy releaser rate in elastic specimens

1. A thin strip (plane stress) with length L and height h clamped at the upper and lower edges with vertical displacement $\pm\Delta$ applied. Crack length = a .

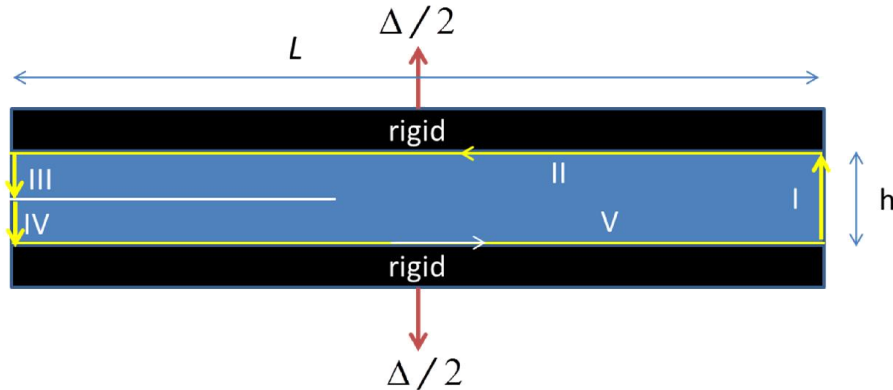


Figure 4d Schematic of a Mode I strip specimen held in rigid grip subjected to prescribed separation.

To evaluate the J integral of the sample in Fig.4d, we use a path consisting of 5 paths indicated by I, II, III, IV and V above. On paths II and V, integral is zero since $n_1 = 0$ and the vertical displacement is independent of position (horizontal displacement = 0 due to clamp boundary condition). Since traction = 0 on paths III and IV, J integral is

$$J_{III+IV} = -2 \int_{0^+}^{h/2} W_3 dy \quad (2.30)$$

where we have made use of symmetry. Note in general W_3 is the strain energy density evaluated on III. It is not zero in general and will vary along the path, depending on the length of the crack a (think of a very short crack, e.g. $a \ll h$). On path I, we have

$$J_I = \int_{-h/2}^{h/2} W_1 dy \quad (2.31a)$$

where W is the strain energy evaluated on this path and in general is a function of position along I. Thus, the energy release rate is:

$$\Gamma = \int_{-h/2}^{h/2} W_1 dy - 2 \int_{0^+}^{h/2} W_3 dy \quad (2.31b)$$

If the crack length $a \gg h$, then $W_3 \approx 0$, we have

$$\Gamma = \int_{-h/2}^{h/2} W_1 dy \quad (2.31c)$$

If in addition, $L - a \gg h$, we move the path I into the specimen to avoid the complicated fields due to the free surface. As long as path I is sufficiently far away from the edge and the crack tip, the horizontal displacement as well as its derivative in the horizontal direction is zero (since the upper and lower edge of the strip is clamped). Since $n_2 = 0$ and $u_{1,1} = \varepsilon_{11} = 0$ on I , the traction term in the J integral on this new path is still zero and the J integral is still equal to the integral of the strain energy density W along the new path. To compute W_1 on this path, we note that the out of plane stresses are zero for a plane stress sample, also

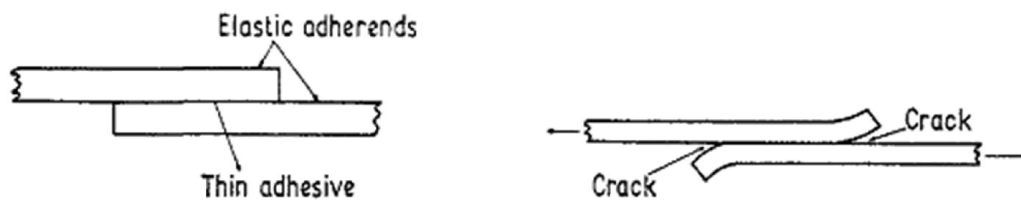
$$u_1 = 0 \Rightarrow \varepsilon_{11} = 0 \Rightarrow \sigma_{11} = -\nu\sigma_{22} \Rightarrow \varepsilon_{22} = \frac{\Delta}{h} = \frac{1-\nu^2}{E} \sigma_{22} \Rightarrow W_1 = \frac{E^*}{2} \left(\frac{\Delta}{h} \right)^2 \quad (2.31d)$$

Substituting (2.31d) into (2.31c) gives the energy release rate, i.e.,

$$\Gamma = \frac{E^*}{2} \left(\frac{\Delta}{h} \right)^2 h, \quad \frac{1}{E^*} = \frac{1-\nu^2}{E} \quad (2.31e)$$

Example 2: Lap-joint test (see Kendall, J. Phys. D: Appl. Phys., vol 8, 1975)

This example is motivated by a recent discussion with Alba Marcellan. The lap-joint test is a widely used test to determine the failure strength of adhesives. In this test, two planar slabs are glued together by a thin adhesive and a force F is applied to pull them apart, as shown in Kendall's figures below:



Figures 4e (on left) and 4f (on right) are taken from Kendall's paper (Kendall, J. Phys. D: Appl. Phys., vol 8, 1975). The two arrows in Figure 4f show the direction of the force F . The top and bottom slabs have thicknesses d_1 and d_2 respectively. The slabs has length L_1 and L_2 respectively. The lab joint has length L . The out of plane width of the slabs are identical and is denoted by b . The material of the slabs is assumed to be identical with Young's modulus E . Figure 4f is an example of an incomplete free body diagram - the specimen is not in equilibrium since there is an unbalance moment or torque (anti-clockwise) of magnitude $F(d_1 + d_2)/2$. This torque must be balanced by the loading system and will

cause rotation of the specimen. Kendall's analysis (and the analysis below) assumes that the bending energy associated with this rotation is small in comparison with the stretching energy.

Before proceeding with our analysis, it should be noted that the Lap-joint test is not a true fracture test since it has no pre-existing crack. The edges of the joints are stress concentrators where crack or cracks can *initiate but there is no guarantee that once initiated, these cracks will grow along the joint*. In fact, a crack can initiate near the joint edge and fracture the slabs instead of running along the joint. In addition, there is no reason why cracks have to propagate symmetrically, as shown in Fig. 4f.

After this brief detour, let's determine the energy release rate of the specimen in Figure 4f using the J integral. In fact, we consider the slightly more general situation³, shown in Figure 4g below.

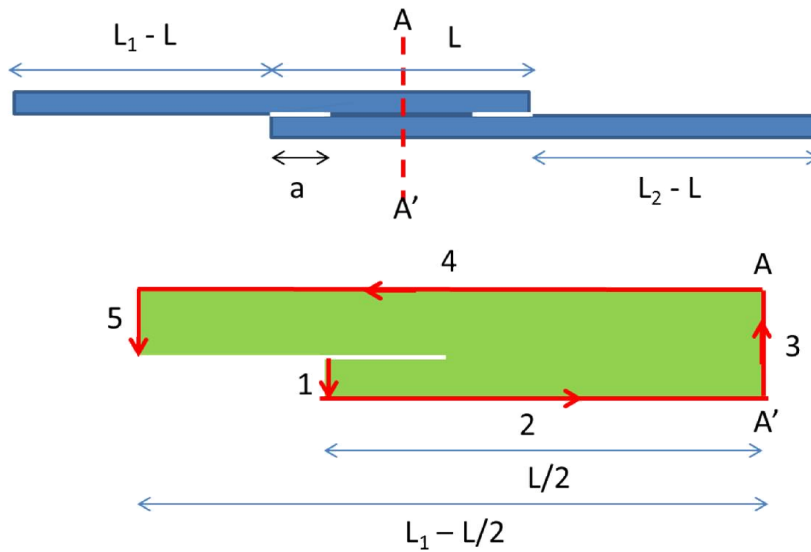


Figure 4g. Schematics of specimen dimension and path to evaluate J integral

Because of the traction free boundary condition, the J integral evaluate along paths 2 and 4 are exactly zero. On path 5, the only non-vanishing component of the traction is $\sigma_{11} = F / bd_1$ (this assumes that the difference in length between the slab and the joint is much greater than the thickness of the slab so that the stress state on this path is that of simple tension). On path 5, $n_2 = 0$,

$$\sigma_{\alpha\beta} n_{\beta} u_{\alpha,1} = \sigma_{11} \varepsilon_{11}, \quad W_5 = \frac{1}{2} \sigma_{11} \varepsilon_{11} \Rightarrow J_5 = \frac{1}{2E} (F / bd_1)^2 h_1 \quad (2.32a)$$

On path III, $n_2 = 0$ and the shear stress σ_{12} is zero by symmetry, so the J integral is

$$J_3 = \int_{-h_2}^{h_1} W_3(y) dy - \int_{-h_2}^{h_1} \sigma_{11} \varepsilon_{11} dy \quad (2.32b)$$

³ Kendall's derivation implicitly assumes that (1) the crack length a is very long in comparison with the thickness of the slab, (2) the length of the slab is very long in comparison with the slab thickness.

where W_3 denote the strain energy evaluated on path 3. The quantities σ_{11} and ε_{11} in (2.32) can be determined if the uncracked joint length $L-2a$ is much greater than the slab thicknesses. In this case the stress state on path 3 is that of uniaxial tension. Specifically, from force balance, the only non-vanishing stress on path 3 is:

$$\sigma_{11} = \frac{F}{b(d_1 + d_2)} \quad (2.32c)$$

As a result, $W_3 = \frac{1}{2}\sigma_{11}\varepsilon_{11}$ on path 3, and using $u_{1,1} = \varepsilon_{11} = \sigma_{11}/E$, we have

$$J_3 = -\frac{1}{2E} \left(\frac{F}{b(d_1 + d_2)} \right)^2 d_1 - \frac{1}{2E} \left(\frac{F}{b(d_1 + d_2)} \right)^2 d_2 \quad (2.32d)$$

Finally, on path 1 (traction free), we have,

$$J_1 = -\int_{-h_2}^0 W_1(y) dy \quad (2.32e)$$

The energy release rate Γ is given by $J_1 + J_3 + J_5$. In particular, for $(L-2a) \gg \max(h_1, h_2)$

$$\Gamma = \frac{1}{2E} \left(\frac{F}{bd_1} \right)^2 d_1 - \frac{1}{2E} \left(\frac{F}{b(d_1 + d_2)} \right)^2 d_1 - \frac{1}{2E} \left(\frac{F}{b(d_1 + d_2)} \right)^2 d_2 - \int_{-h_2}^0 W_1(y) dy \quad (2.32f)$$

For short cracks, W_1 is not zero and is difficult to compute. However, if a is sufficiently long then $W_5 \approx 0$; for this case the last term in (2.32f) can be set to zero, and the energy release rate given by (2.32f). After some simple algebra, it is

$$\Gamma = \frac{1}{2E} \left(\frac{F}{b} \right)^2 \frac{1}{d_1} \left[1 - \frac{d_1}{(d_1 + d_2)} \right] \quad (2.32g)$$

Crack growth occurs when the applied force F satisfies the fracture condition $\Gamma = G_{IC}$. This gives the critical force for crack growth:

$$\Gamma = \frac{1}{2E} \left(\frac{F}{b} \right)^2 \frac{1}{d_1} \left[1 - \frac{d_1}{(d_1 + d_2)} \right] = G_{IC} \Rightarrow F = b \sqrt{2E \frac{d_1(d_1 + d_2)}{d_2} G_{IC}} \quad (2.32h)$$

This result is identical to the expression of critical force given by Kendall. Note that if the crack is short, then (2.32f) implies that the applied energy release rate is lower than given by (2.32g) (since $W_1 \geq 0$), so a larger force is needed to grow the crack.

Cohesive zone Model: an introduction

SSY enables one to rationalize the divergence in stress and strain fields. However, in order to determine the RHS of the equation,

$$K = K_c \Leftrightarrow J = G_c$$

it is necessary to model the fracture processes. In older literature it is common to introduce a characteristic length scale directly ahead of the crack tip and imposed a fracture criterion such as a critical strain or critical stress criterion at this length. A more systematic way is to use a cohesive zone model to describe the separation process directly ahead of the crack tip. In the following we consider the more general case of an interface between two different solids, although the focus of these lectures is on cracks in homogeneous solids. Since its introduction by Barenblatt in 1962 [5], cohesive zone models have been used to study a wide variety of physical phenomenon, for example, crack growth along a prescribed plane in elastic-plastic and viscoelastic materials, adhesive contact of non-conforming surfaces, frictional sliding and earthquakes, sintering of polymeric particles, crazing in polymer glass, adhesion, fiber bridging and debonding in composite materials and stability of interfaces.

The number of research papers using cohesive zone models to study different physical phenomenon has been increasing rapidly in the past ten years. However, far less attention has been paid to understanding cohesive models from the point of view of constitutive modeling. For example, there have been very few discussions on the deficiencies and limitations of cohesive zone models currently used in the literature. The concept of interfacial displacement or displacement discontinuity in the continuum description is often misunderstood. For example, *it is often assumed that the interface displacements that enter the constitutive model are identical to the experimental interfacial separations, whereas in reality these two quantities can differ significantly.* In this lecture, I attempt to explain these fundamental concepts. For a more detail discussion on this subject, see reference [11].

2 Constitutive Relation or Cohesive zone model

2.1 Continuum 'Point' on an Interface

The existence of a constitutive relation requires the concept of a continuum 'point'. A continuum 'point' is a region of the interface between the solids with characteristic dimension P in the plane of the interface. It may include *a thin layer of the adjacent solids of characteristic size H* in a direction normal to the interface. The size of P and H must be negligible comparable to all relevant geometric dimensions L in the continuum problem. Figure 5 shows a region of a solid that include a planar interface that may undergo opening or slip. The 'point' is assumed to include many microscopic features (see Fig. 6 for an example). These microscopic features may include molecular chain scission or pull-out in polymers, asperities that deform and fracture in frictional sliding, micro-void formation, growth and coalescence of these voids in metals and elastomers, drawing and formation of craze fibrils in polymer glasses, slipping at the fiber/matrix interface, breaking of fibers and fiber pull-out in a fiber-reinforced composites. Smaller features can also be represented by the 'point', e.g. intermolecular or interatomic interactions such as Van der Waals, hydrogen and ionic bonding. In general, these micro-

nano-mechanical elements have a wide range of characteristic sizes (m, h) and a continuum point may include many of these mechanisms. For example, $m, h \approx \text{\AA}$ for interatomic interactions, $m \approx nm$ for craze fibrils and dislocations, $m \approx \mu m$ or higher for voids, $h \approx \mu m$ for crazes and $h \approx mm$ for fiber pull-out. Thus, for the continuum description to be legitimate, a hierarchy of size scales is implicit, such that $L \gg P \gg m, h$. In addition, over a wide range of length scales, the constitutive relation must be independent of the size of the continuum point.

In Barenblatt's theory, separation of two surfaces is opposed by interatomic or intermolecular forces so that the traction across the cohesive zone is the gradient of an interatomic potential. In this case, $m, h \approx \text{\AA}$, and the value of fracture toughness approaches twice the surface energy. For most material systems this theory is too simplistic, since, even in nearly ideal-brittle materials such as glass and mica, the fracture toughness is much higher than twice the surface energy. This is because for most materials, the interatomic forces required for separation are much higher than those required to initiate some form of damage (e.g. cavitation, plastic flow, or crazing). Therefore, the material invariably suffers some form of inelastic deformation near the crack tip, resulting in much greater energy dissipation. Even in the few cases where fracture toughness does indeed equal twice the surface energy, as in separation of carefully-prepared elastomers, the cohesive stress is much smaller than would be expected on the basis of intermolecular interactions between continuous bodies. This fact is typical; the characteristic stress (displacement) to separate the interface is much smaller (larger) than predicted on the basis of intermolecular forces.

Consider, for example, the fracture of rubber. Based on the typical number of chains ($\approx 10^{18} / m^2$) that across a fracture plane and the energy needed to break a chemical bond ($\approx 400 \text{kJ/mole}$), the surface energy should be about $1-2 \text{ J/m}^2$. Experimental values of fracture energies, however, range from 10 to 1000J/m^2 [6]. The stress needed to completely separate the interface is on the order of GPa, which is at least 4 orders of magnitude higher than the small strain elastic modulus ($E \approx 1 \text{MPa}$) of a typical elastomer. Crack growth can occur by at least two mechanisms: in the first, the highly stretched polymer chains directly ahead of the crack tip break. As pointed out by Lake and Thomas [6], since all the bonds in a chain are stretched to their breaking point, when one of the bonds breaks, the entire chain relaxes to zero load and all of the stored elastic energy in the chain is lost⁴. The energy dissipation is thus proportional to number of bonds in a chain between crosslinks. For long chains, the characteristic interfacial displacement required to separate the interface is on the order of microns. Cracks can also grow by linking of microvoids ahead of the crack tip. In elastomers, a typical stress for rapid growth of micro-voids is on the order of ($E \approx 1 \text{MPa}$), much smaller than the stress required to break bonds. In addition, blunting of the crack tip suggests that the effective size and the thickness of the cohesive zone can be much greater than atomic dimensions. The same issue also exists in metallic systems, where the theoretical cohesive stress based on intermolecular potential is typically much higher than the yield stress. Thus, the plastic zone engulfing the crack tip will continue to grow in size until strain hardening eventually produce a high enough stress to break bonds. For crazes in glassy

⁴ Lake and Thomas did not give any details on the mechanism of energy loss.

polymer, the thickness of the cohesive zone is typically on the order of microns. The thickness of the continuum ‘point’ in the bridging zone of fiber-reinforced composites can be on the order of millimeters.

2.2 Definition of interfacial displacements

The discussion above shows that the thickness H of an interface continuum ‘point’ can be much larger than m, h , which are characteristic length scales of the microstructure. The following question naturally arises, what is an appropriate definition of interfacial displacement? The insert in Figure 5 shows two material points separated by a distance $H \gg h$ on opposite sides of a planar interface. Let \vec{u} be the separation between these two material points with component u_1 normal to the interface and components u_2 and u_3 in its plane. Let \vec{u}_0 be the separation that would be predicted between these two points based on bulk deformation of the solids if subjected to the same remote state of stress. Then, we define the displacement $\vec{\delta} = \vec{u} - \vec{u}_0$ as the interface displacement of the cohesive zone and components δ_1 as the normal and δ_2, δ_3 as the slip displacements. That is, the cohesive zone displacements are the *excess relative over that which would be predicted by the bulk deformation of the solids*. (We pick H to be sufficiently large compared to h but still sufficiently small compared to L so that stresses and strains locally are homogeneous prior to introduction of the interface and so that the displacements, so defined, are independent of the choice of H . For the special case where the interface deformation is highly localized, such as that of a craze, H can be taken to be h .)

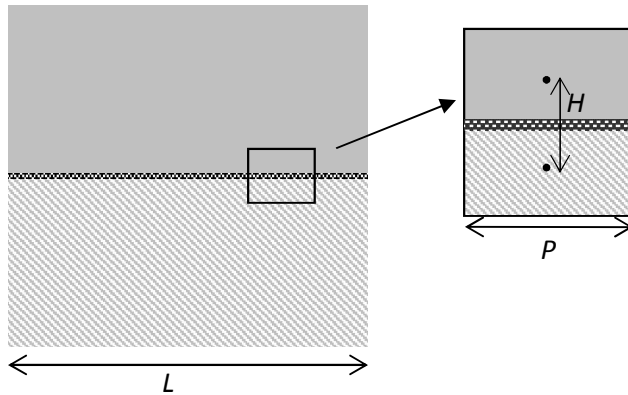


Figure 5. Schematic drawing of a continuum point. L is a characteristic length scale of the continuum problem (e.g. specimen size, crack length, etc). P and H denote the size scale of the continuum point. The continuum stress and strains fields are approximately homogeneous over the length scales P and H .

This definition implies that the opening or slip displacements observed in the laboratory can be substantially different than the opening or slip displacements used in the cohesive model. As an example, consider crazes, which are planar crack-like defects in glassy polymers [7]. However, unlike cracks, crazes are load-bearing, since their surfaces are bridged by many fine fibrils with diameters ranges from 5 to 30 nms (see Fig 6). As the craze grows in thickness this fibril structure may break

down, leading to large voids which eventually grow to become cracks of a critical size. Experiments have conclusively demonstrated that crazes in air increase in thickness by drawing material from a thin ($\approx nm$), strain softened layer at the craze-bulk interface into the fibrils. Since the fibril structure cannot withstand shear, $\delta_2 = \delta_3 \approx 0$. As a result, the direction of the tensile stress is always normal to the craze surface and the craze thickens primarily in the direction of its fibrils.

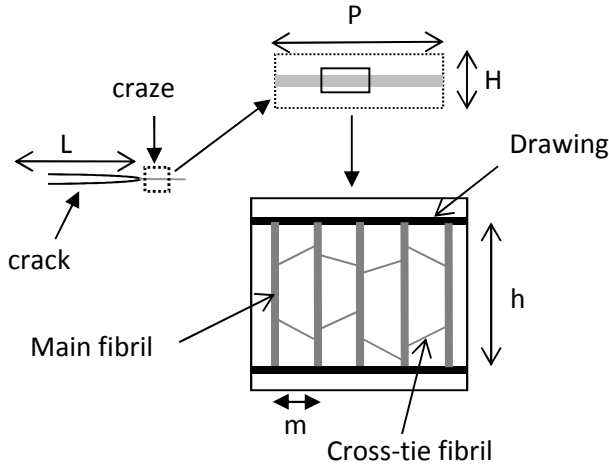


Figure 6: An example of the micro-structures inside a craze. P , H denote the size of the continuum point.

To illustrate the procedure of computing the interfacial displacement δ_1 for a craze, consider Fig. 7a,b where a comparison is made between the normal displacement of two material points induced by the bulk deformation of the polymer (elastic or inelastic) and the final deformation of the same material points after the craze has formed. The separation of these two points before deformation is denoted by H_o . The separation of these points after the craze has formed is H . Let ρ_o be the density of the homogenously deformed bulk material in Fig. 7a, and let ρ be the density of the craze and bulk material in Fig. 7b. In general, ρ is a function of the distance along the y axis (the y direction is perpendicular to the craze interface), and the planar interface is the xz -plane. Since one can reasonably assume that there is no excess lateral strain due to crazing, we have

$$\rho_o H_o = \int_0^H \rho(y) dy \equiv \bar{\rho} H \quad (2.33a)$$

by mass conservation, where $\bar{\rho}$ is the average density of the crazed material. The interface displacement is, by definition,

$$\delta_1 \equiv H - H_o \quad (2.33b)$$

Substituting (2.33a) into (2.33b), we have

$$\delta_1 = H \left(1 - \frac{\bar{\rho}}{\rho_o} \right) \quad (2.33c)$$

For crazes, the craze-bulk interface is very sharp ($\approx 10nm$) so a *convenient choice* is to select the material points so that $H = h$, where h is the visible thickness of the craze (e.g. in a transmission electron micrograph). The interface displacement is

$$\delta_1 = h \left(1 - \frac{\rho_c}{\rho_o} \right) \quad (2.33d)$$

where ρ_c is the average mass density in the craze⁵. *The above definition of δ_1 is independent of the distance H_o of the two material points, as long as H_o is large enough to include all the details of fibrillation.* This definition is the same as an early expression of Kramer [6]. For crazes in Polystyrene, $\rho_c / \rho_o \approx 0.2$ so that *the continuum normal displacement is about 80% of the visible craze thickness.*

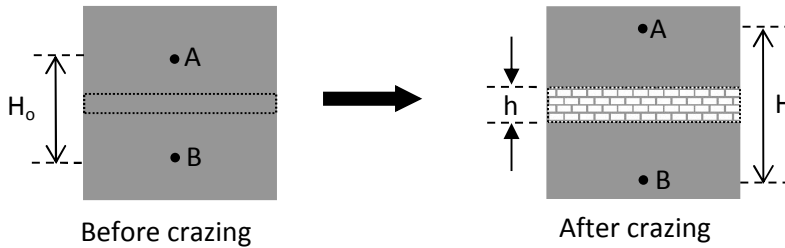


Figure 7. (7a) Continuum point before crazing occurs. The craze material is highlighted by the dotted lines. (7b) After crazing, the material inside the box highlighted in Fig.(7a) increases its thickness to h and becomes less dense. The two black dots denote two points A, B before and after crazing.

In a very different application, we point out that there is some ambiguity in the published literature on the appropriate definition of interface displacement to model crack bridging in fiber reinforced composites. For example, the continuum opening displacement in crack bridging models is the additional displacement of a remote material point of a cracked composite (i.e., the matrix is fully cracked) over that which would result in an uncracked composite under the same loading. This procedure is entirely consistent with our definition of interfacial displacement.

⁵ Since the effective Young's modulus of the crazed material E_c is less than that of the bulk polymer, E , we should include the difference in elastic deformation, a factor of $h\sigma_c(E_c^{-1} - E^{-1})$ in (2.33b), where σ_c is the crazing stress. However, since σ_c/E is on the order of 10^{-3} , this factor is much smaller than the RHS of (2.33b), and so it is neglected.

Many cohesive zone models have an initial hardening branch, that is, the interfacial displacements are non-zero for any applied traction, no matter how small. A very simple example of a linear hardening model is to consider a thin layer of soft elastic material of uniform thickness h perfectly bonded between two identical homogeneous, isotropic, linear elastic plates with Young's modulus E and Poisson's ratio ν . For simplicity, let us consider a plane stress problem (e.g. a thin sheet of material between two identical plates). Let E_L and ν_L denote the Young's modulus and Poisson's ratio of the layer. If h is much smaller than the crack tip radius, this layer can be treated as a cohesive zone. In the absence of the layer, the two points A, B (see Fig. 7a,b) displace by the amount of

$$\sigma H_o / E, \quad (2.34a)$$

where σ is the normal stress applied at distances far from the layer (see Fig. 8). Assuming that the lateral contraction of the soft layer is the same as that of the two large identical plates, the displacement of A, B, in the presence of the layer is

$$\frac{\sigma}{E}(H_o - h) + \frac{\sigma h}{E_L} \left[1 - \nu_L^2 \left(1 - \frac{E_L \nu}{E \nu_L} \right) \right] \quad (2.34b)$$

By definition, the excess displacement or opening interface displacement δ is the difference between (2.34b) and (2.34a), that is,

$$\delta = \frac{\sigma h}{E_L} \left[1 - \nu_L^2 \left(1 - \frac{E_L \nu}{E \nu_L} \right) \right] - \frac{\sigma h}{E} \quad (2.34c)$$

Note that the result is *independent* of H_o and the interface displacement *vanishes* if the two materials are identical. This hypothetical model has a linear 'hardening' branch where the interface displacement δ is directly proportional to the normal traction σ . In a more realistic model, the hardening branch is usually followed by a softening branch, where σ decreases with increasing δ . The behavior of the softening branch depends on the failure characteristic of the layer. For example, if the layer fails in a brittle way (e.g. by the propagation of a single crack), then softening occurs very rapidly. However if the layer fails by cavitation⁶, then the range of δ where softening occurs can be very large.

As demonstrated by the above example, *our definition of interfacial displacement implies that inter-atomic models of interface cohesion or decohesion should have no linear hardening branch since the linear elastic behavior of the continuum point is indistinguishable from the bulk behavior.*

⁶ Cavitation is more likely to occur if the layer were loaded in plane strain and $E \gg E_L$, $\nu_L \approx 0.5$, for example, if the plates were blocks of glass and the layer were replaced by a thin sheet of rubber or soft elastic gel.

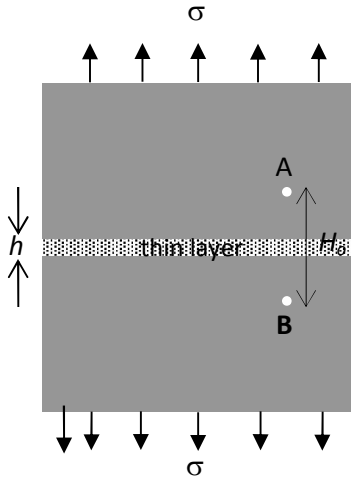


Figure 8. A thin elastic layer sandwiched between two linearly elastic plates.

2.3 Variables in cohesive zone model

The primary mechanical variables of interest are the normal traction T_1 (traction component in the direction normal to the interface), the shear tractions T_2 , T_3 and the interface displacement vector $\vec{\delta} = (\delta_1, \delta_2, \delta_3)$ defined above. To define these displacements and tractions we need first to define a cohesive plane. *A full mechanical description could conceivably include other deformation variables such as the relative rotation of the two surfaces and the in-plane strain in the two solids.* For example, the nucleation and growth of micro-voids ahead of the crack tip can be significantly affected by the in-plane strain, especially if crack blunting occurs since void nucleation and growth are known to be very sensitive to stress triaxiality.

A reasonable general constitutive model for the interface or cohesive zone model can be written in the form of a relation as follows:

$$\mathbf{G} \left\{ \vec{T}(t), \mathbf{F} \left[\vec{\delta}(t'), -\infty \leq t' \leq t \right] \right\} = \mathbf{0} \quad (2.35a)$$

In the above \mathbf{F} is a vector function which depends on the history of the displacement vector that is related to the traction vector $\vec{T} \equiv (T_1, T_2, T_3)$ through the vector relation

$$\mathbf{G}(\vec{T}, \mathbf{F}) = \mathbf{0} \quad (2.35b)$$

2.4 Definition of cohesive zone, cohesive zone tip and Crack tip

The cohesive zone, cohesive zone front and crack front can be defined in a formal way. At any time t , the cohesive zone consists of all points on the interface such that $\delta \equiv |\vec{\delta}| > 0$. A cohesive zone

front is the boundary points (in general a space curve) between two adjacent regions on the interface where at least one of the interface displacements goes from identically zero in one region to having non-zero values in the other. This definition allows for multiple cohesive zone fronts within a cohesive zone and its boundaries. For example, it is possible to have part of the cohesive zone deform in the pure opening mode (or in a pure sliding mode), whereas the rest of the cohesive zone deforms in both opening and sliding mode. In general, true cohesive zone front(s) exist only for constitutive models that allow $\delta_i = 0$ for *some* i and for some *nonzero* traction histories. In the absence of crack healing or internal fluid pressure, we define a crack zone as the part of the interface that *belongs to a cohesive zone*; however, material points in this region can bear no load for the current and all possible future configurations, that is $\vec{T} \equiv 0$ for all $t' \geq t$. A crack front is defined as the boundary points between a crack zone and a cohesive zone. We will illustrate these ideas shortly with some simple examples.

Although it is possible to construct examples where the displacement normal to the interface is negative (e.g. a soft interface layer under compression), it is common to enforce $\delta_1 \geq 0$ at all times. In this work, we will adopt the convention that contact occurs when $\delta_1 = 0$, and friction force must be taken into account if $T_1 < 0$. *In cohesive zone models, preexisting cracks or cracks that are artificially introduced into the interface which do not satisfy a fracture criterion consistent with the cohesive zone model, cannot be considered as part of the interface and hence cannot be described by the model.* Descriptions of these cracks must be captured by boundary conditions. We will call these types of cracks *preexisting cracks*.

Figure 9 shows some simple examples where $T_2 = T_3 = \delta_2 = \delta_3 = 0$, that is, the interface is constrained to open in the direction of its normal. The cohesive zone tip and the crack tip are well defined for the cohesive zone model in Fig. 9a. At the cohesive zone tip, the normal traction $T = T_1$ is exactly $\sigma_0 > 0$. Crack tips are defined by the condition $\delta = \delta_c$.

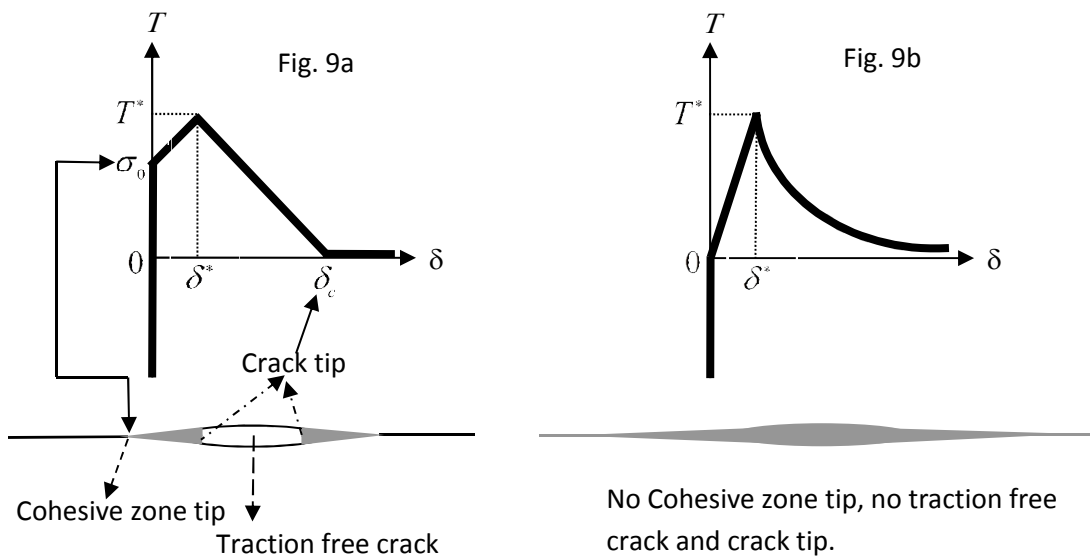


Figure 9 (a) A cohesive zone model where cohesive zone tips and crack tips are well defined. (b) A cohesive zone model where neither the cohesive zone tips nor crack tips exist.

2.5 Constitutive Relation based on Potential Function

A simple and widely used constitutive relation is the reversible cohesive zone model introduced by Needleman [8]. Let a displacement $\vec{\delta} = (\delta_1, \delta_2, \delta_3)$ be imposed on a continuum point. Denote the resulting traction on this point by $\vec{T} = (T_1, T_2, T_3)$. The work done by the cohesive traction per unit area from $\vec{\delta}_a$ to $\vec{\delta}_b$ is

$$\int_{\vec{\delta}_a}^{\vec{\delta}_b} \vec{T} \cdot d\vec{\delta}. \quad (2.36)$$

This integral is *path dependent* unless \vec{T} is the gradient of a potential or work function $\Phi(\vec{\delta})$, i.e.,

$$T_i = \Phi_{,i} \equiv \partial\Phi / \partial\delta_i \quad (2.37)$$

Equation (7) is the fundamental equation governing the work function approach. The work function, $\Phi(\vec{\delta}) = \text{constant}$ represents a family of surfaces in the space of cohesive opening displacements. Geometrically, eq (7) states that the traction vector is normal to these equi-potential surfaces.

An example of such a work function in two dimensions (i.e., $\delta_3 = 0$) is [8]:

$$\Phi(\delta_1, \delta_2) = W_1 + W_1 \left(1 + \frac{\delta_1}{\delta_1^*} \right) e^{-\frac{\delta_1}{\delta_1^*}} \left((q-1) - q e^{-\frac{\delta_2^2}{(\delta_2^*)^2}} \right) \quad (2.38a),$$

where $q = W_2 / W_1$. W_1 is the energy needed to separate a unit area of the interface in pure tension (commonly referred to as the Intrinsic work of adhesion) and W_2 is the energy needed to fail the interface in pure shear and δ_i^* ($i=1,2$) are material parameters that represent characteristic opening distances over which the cohesive tractions act. Using (2.37), the traction vector is

$$T_1 = \frac{W_1 \delta_1}{(\delta_1^*)^2} e^{-\frac{\delta_1}{\delta_1^*}} \left(1 - q \left(1 - e^{-\frac{\delta_2^2}{(\delta_2^*)^2}} \right) \right) \quad (2.38b)$$

$$T_2 = \frac{2W_2 \delta_2}{(\delta_2^*)^2} \left(1 + \frac{\delta_1}{\delta_1^*} \right) e^{-\frac{\delta_1}{\delta_1^*}} e^{-\frac{\delta_2^2}{(\delta_2^*)^2}} \quad (2.38c)$$

A one-dimensional work function $\phi(\delta_1)$ can be extended to the three dimensional case by defining $\Phi(\delta_1, \delta_2, \delta_3) \equiv \phi(\delta_e)$ where $\delta_e \equiv \sqrt{\delta_1^2 + \beta(\delta_2^2 + \delta_3^2)}$ and $\beta > 0$ is a material constant.

Since the failure of the interface is defined by its inability to support traction, (2.38b) and (2.38c) imply that the interface fails if any one of the following conditions is satisfied:

$$i) \quad \delta_1 \rightarrow \infty \quad (2.39a)$$

$$ii) \quad \delta_1 = 0 \text{ and } |\delta_2| \rightarrow \infty \quad (2.39b)$$

Note that except for a set of measure zero, i.e., if the interface were loaded in pure shear, failure in shear must be accompanied by failure in tension.

Equations (2.38a,b,c) illustrate three features of cohesive models that are widely used:

(a) The traction vanishes as $\vec{\delta} \rightarrow \vec{0}$ (Initial hardening, cohesive front not defined),

(b) Non-zero traction for all finite $\delta \equiv |\vec{\delta}|$ (crack front not well-defined). Note that the traction vanishes much faster than δ^{-1} as $\delta \rightarrow \infty$,

(c) The work to fail a unit area of the interface is always \mathcal{W}_1 , independent of the loading direction. The only exception is when the interface is loaded in pure shear. In this case the work is \mathcal{W}_2 . In the following we examine each of these features in detail.

2.6 Hardening vs Rigid models

Cohesive zone models in which the traction vanish smoothly as $\vec{\delta} \rightarrow \vec{0}$ will be defined as *hardening models*. In hardening models, cohesive zone fronts cannot exist in any finite structures under load (see definition of cohesive zone front earlier). In a finite element model, hardening cohesive zone models can lead to softening of bulk behavior. Another interesting but less well known result is that material interpenetration will always occur if a hardening cohesive zone model is used to study the growth of a preexisting crack loaded in Mode I. It should be noted that material interpenetration is penalized in Needleman's model by the term $\delta_1 \exp(-\delta_1 / \delta_1^*)$ in (2.38b). By making δ_1^* very small, very large normal compressive traction results as δ_1 become negative.

Thus, a cohesive zone model with a hardening branch has the unpleasant features:

1. material softening
2. material interpenetration

Cohesive zone fronts are well defined in “Rigid” cohesive models such as the classical Dugdale-Barenblatt (DB) model which was used to model plane stress Mode I fracture of mild steel. This model can be extended to include shear deformation. The potential associated with the generalized Dugdale-Barenblatt (GDB) model is

$$\Phi = \sigma_o \delta_1 + \tau_o |\delta_2| + \tau_o |\delta_3|, \quad (2.40)$$

where σ_o, τ_o are the critical cohesive stresses to open and slip the interface respectively. To prevent material interpenetration, the potential function is defined in the half space $\delta_1 > 0$. According to (2.37), interface displacements can occur if

$$T_1 = \sigma_o \quad \delta_1 > 0 \quad (2.41a)$$

$$T_i = \pm \tau_o \quad \delta_i > 0 (+), \delta_i < 0 (-) \quad , i = 2, 3 \quad (2.41b)$$

In analogy with classical plasticity, the planes $T_1 = \sigma_o$ and $T_i = \pm \tau_o$ can be viewed as a “yield” surface in traction space (T_1, T_2, T_3) . A traction vector that is inside the yield surface cannot cause interfacial displacement. Note that the origin $\vec{\delta} = \vec{0}$ is a point of where the traction vector is not uniquely defined. Also, the GDB model yield surface is not smooth, it has corners at the vertices of the rectangle defined by the intersections of the lines in (2.41a,b).

Specifically, a “Rigid” cohesive model must formally satisfy the condition

$$\lim_{\vec{\delta} \rightarrow \vec{0}^+} \vec{T} \neq \vec{0}. \quad (2.42)$$

The notation $\vec{\delta} \rightarrow \vec{0}^+$ implies that the limit is taken with $\delta \equiv |\vec{\delta}| > 0$. Note that $\lim_{\vec{\delta} \rightarrow \vec{0}} \vec{T}$ does not exist in the usual mathematical sense since the traction vector is not a continuous function of the interface displacement vector at zero. In this work, the existence of $\lim_{\vec{\delta} \rightarrow \vec{0}} \vec{T}$ means that the traction vector will approach a unique value *given any smooth path approaching the origin in displacement space with $\delta > 0$* , although each path will, in general, produce a different limit. We further assume that this limit depends only on the tangent of the path as it approaches $\delta = 0$; in other words, *the limiting value of traction is the same for all smooth curves entering $\delta = 0$ with the same slope*. The resulting potential surface defined by this limiting process in stress space is called a “yield” surface, in analogy with classical plasticity. For a perfectly rigid cohesive zone model, the traction vector must lie inside or on the yield surface. The interface displacement vector is identically zero for any traction vector inside the yield surface. Plastic flow is equivalent to the motion of the interface. Equation (2.37) implies that interface motion in a rigid cohesive zone model is possible if and only if the traction vector is normal to equipotential surfaces in displacement space.

For example, if the potential function is given by:

$$\Phi = A\sqrt{\delta_1^2 + \beta(\delta_2^2 + \delta_3^2)} \quad \beta > 0 \quad (2.43)$$

where A and β are positive constants. For non-trivial displacement, the traction is

$$\vec{T} = \frac{A}{\sqrt{\delta_1^2 + \beta(\delta_2^2 + \delta_3^2)}} (\delta_1, \beta\delta_2, \beta\delta_3) \quad (2.44)$$

This model is perfectly rigid since the limit of \vec{T} as $\vec{\delta} \rightarrow \vec{0}$ is in general a non-zero vector (see below). Furthermore, (2.44) implies that

$$A^{-2}T_1^2 + (A^2\beta)^{-1}(T_2^2 + T_3^2) = 1 \quad (2.45)$$

Equation (2.45) implies that the yield surface is an ellipsoid of revolution with semi-axis A and $A\sqrt{\beta}$. For the special case of $\beta=1$, the yield surface is a sphere of radius A . A path in displacement space corresponds to a path on the yield surface. For example, consider a straight line path $\delta_2 = a\delta_1, \delta_3 = b\delta_1$ in displacement space, where a, b are positive numbers. The image of this path on the yield surface can be obtained using (2.45). For this special case, the path in stress space collapses to a single point on the yield surface, i.e., $\vec{T} = \frac{A}{\sqrt{1 + \beta(a^2 + b^2)}} (1, \beta a, \beta b)$. Thus, the interface continues to deform under this constant traction, in analogy with a rigid plastic material.

It is possible to construct rigid models in which the yield surface evolves with interface motion. For example, consider

$$\Phi = \sqrt{\delta_1^2 + \beta(\delta_2^2 + \delta_3^2)} \chi(\delta_1, \delta_2, \delta_3) \quad (2.46)$$

where χ is a smooth function of its arguments. In particular, $\chi(0,0,0) = A > 0$. For this case, the initial yield surface is still given by (2.45), but subsequent yield surfaces are determined by the behavior of χ . As an example, consider

$$\Phi = \sqrt{\delta_1^2 + \beta(\delta_2^2 + \delta_3^2)} e^{-\delta_1 - (\delta_2^2 + \delta_3^2)} \quad (2.47)$$

Equation (2.47) implies that the yield surface shrinks with interfacial motion. It can be verified easily that the traction decreases with the size of the yield surface and that failure of the interface occurs when the yield surface shrinks to the point $\vec{\delta} = \vec{0}$.

It is well known that the interface fracture toughness of most bimaterial systems is dependent on the applied phase angle. Potential functions that has bounded energy as $|\vec{\delta}| \rightarrow \infty$ (see paragraph after equation 2.39b) in general cannot predict such dependence, unless the material outside the

cohesive zone undergoes *inelastic* deformation. In this case, the size of the plastic zone depends on both the cohesive model and the plastic flow rule. As a result, the energy dissipated as the crack advances depends on the loading direction, even though the intrinsic work to separate the interface does not. This approach has been pursued by Tvergaard and Hutchinson [9,10]. However, there are physical systems where inelastic deformation is primarily confined to a thin layer of material along interfaces, for example, friction sliding and shear deformation zone in polymers. Furthermore, there is no intrinsic reason which suggests that the work to fail an interface must be independent of the loading direction.

It is possible to construct potentials with bounded energy that has directional interfacial fracture energies. For example, consider the potential

$$\Phi(\delta_1, \delta_2) = W_{II} \tanh\left(\frac{\alpha\bar{\delta}_1^2 + \bar{\delta}_2^2}{1 + \bar{\delta}_1^2}\right), \quad (2.48)$$

where α is defined by $\tanh \alpha \equiv W_I / W_{II}$. In (18), the displacements are normalized by some appropriate characteristic length δ^* , i.e., $\bar{\delta}_i = \delta_i / \delta^*$. Note

$$\Phi(\delta_1 = 0, \delta_2 \rightarrow \infty) = W_{II} \quad (2.49a)$$

$$W_I \equiv \Phi(\delta_1 \rightarrow \infty, \delta_2 = 0) = (\tanh \alpha)W_{II} = W_I \quad (2.49b)$$

For proportional loading in displacement space, i.e., if $\delta_1 \rightarrow \infty$ and $\delta_2 \rightarrow \infty$ along the line $\delta_1 / \delta_2 = b$, then

$$\Phi(\delta_1 \rightarrow \infty, \delta_2 \rightarrow \infty) = W_{II} \tanh\left(\frac{\alpha b^2 + 1}{b^2}\right) \quad (2.50)$$

The tractions are:

$$T_1 = W_{II} \frac{2\bar{\delta}_1(\alpha - \bar{\delta}_2^2)}{\delta_*(1 + \bar{\delta}_1^2)^2} \operatorname{sech}^2\left(\frac{\alpha\bar{\delta}_1^2 + \bar{\delta}_2^2}{1 + \bar{\delta}_1^2}\right) \quad (2.51a)$$

$$T_2 = W_{II} \frac{2\bar{\delta}_2}{\delta_*(1 + \bar{\delta}_1^2)} \operatorname{sech}^2\left(\frac{\alpha\bar{\delta}_1^2 + \bar{\delta}_2^2}{1 + \bar{\delta}_1^2}\right) \quad (2.51b)$$

Equations (2.51a,b) imply that if $\delta_1 \rightarrow \infty$ and $\delta_2 \rightarrow \infty$ along the line $\delta_1 / \delta_2 = b$, the magnitude of the traction vanishes like $|\bar{T}| \approx 1/\delta$, where $\delta \equiv \sqrt{\delta_1^2 + \delta_2^2}$. In general, the work to fail a unit area of the interface depends on the rate for which $\delta_1 \rightarrow \infty$ and $\delta_2 \rightarrow \infty$. For example, if $\delta_1 = \beta\delta_2^2$ and $\delta_2 \rightarrow \infty$, then

$$\Phi(\delta_1 \rightarrow \infty, \delta_2 \rightarrow \infty) = W_I \quad (2.52)$$

We now show that the traction associated with potentials which allow directional fracture energies must decay as δ^{-1} as $\delta \rightarrow \infty$. To demonstrate this result, we employ a polar description of the work function, i.e., $\Phi = \Phi(\delta, \theta)$, where $\delta \equiv \sqrt{\delta_1^2 + \delta_2^2}$ and $\theta \equiv \tan^{-1}(\delta_2 / \delta_1)$. In polar coordinates, the tractions are

$$T_\delta = \partial\Phi / \partial\delta, \quad T_\theta = \frac{1}{\delta} \frac{\partial\Phi}{\partial\theta} \quad (2.53)$$

(T_δ, T_θ) is related to (T_1, T_2) by usual vector transformation:

$$T_\delta = T_1 \cos \theta + T_2 \sin \theta, \quad T_\theta = (-T_1 \sin \theta + T_2 \cos \theta) \quad (2.54)$$

The displacement $(\delta_\delta, \delta_\theta)$ is related to (δ_1, δ_2) by a similar expression. The requirement that the fracture toughness depends on the loading direction implies that $\Phi(\delta \rightarrow \infty, \theta) \rightarrow G(\theta)$. Therefore, a necessary condition for the work function to have different interfacial energies for different loading directions is $dG/d\theta \neq 0$. If this is the case, then (2.53) implies that T_θ must vary as δ^{-1} as $\delta \rightarrow \infty$. Another way to understand this result is to note that the work done by the traction from $\vec{\delta}_a$ to $\vec{\delta}_b$ is

$$\Phi_{ab} = \int_{\vec{\delta}_a}^{\vec{\delta}_b} (T_R d\delta_R + T_\theta d\delta_\theta). \quad (2.55)$$

Let $\vec{\delta}_a$ and $\vec{\delta}_b$ lie on a very large circle with radius δ . Since $G(\theta)$ is a non-constant function, Φ_{ab} cannot be zero. Since $\vec{\delta}_a$ and $\vec{\delta}_b$ lie on a circular path, $d\delta_R = 0$ and $d\delta_\theta = \delta d\theta$. This implies that $\Phi_{ab} = \delta \int_{\theta_a}^{\theta_b} T_\theta d\theta$. Thus, for bounded non-zero values of Φ_{ab} , $T_\theta \propto 1/\delta$ as $\delta \rightarrow \infty$. Also, the first equation in (2.53) implies that T_δ must decay faster than $1/\delta$ as $\delta \rightarrow \infty$. This result, together with (24), shows that T_1, T_2 vanishes as $1/\delta$ as $\delta \rightarrow \infty$.

Why don't we use this type of potentials? The problem is that potentials with directional dependent interface energies always violate steady state crack growth under small scale yielding (SSY) conditions. To see this, consider a semi-infinite plane strain crack lying along the negative real axis. The material is assumed to be homogeneous, isotropic and linearly elastic with Young's modulus E . The SSY boundary condition is

$$\sigma_{ij}(r \rightarrow \infty, \theta) = \frac{K_I}{\sqrt{2\pi r}} f_{ij}^I(\theta) + \frac{K_{II}}{\sqrt{2\pi r}} f_{ij}^{II}(\theta). \quad (2.56)$$

where (r, θ) is a polar coordinate system at the crack tip, $f_{ij}^I(\theta)$ and $f_{ij}^{II}(\theta)$ are universal dimensionless functions describing the angular variation of the stresses. To satisfy SSY, the stresses due to the cohesive zone must be small compared to the applied field (2.56) as $r \rightarrow \infty$. SSY and steady state crack growth implies that interfacial displacement in the far field must be given by

$$\delta_1 \propto K_I \sqrt{-x} / E \text{ and } \delta_2 \propto K_{II} \sqrt{-x} / E \text{ as } x \rightarrow -\infty \quad (2.57)$$

On the other hand, our previous analysis shows that T_θ is proportional to $1/\sqrt{\delta_1^2 + \delta_2^2}$ as $\sqrt{\delta_1^2 + \delta_2^2} \rightarrow \infty$. According to (2.57), T_θ must vary as $1/\sqrt{-x}$ as $x \rightarrow -\infty$. This would mean that the normal cohesive traction is the same order of magnitude as the applied stresses at infinity – a contradiction to the assumption of SSY.

Thus, potentials defined in the half space $\delta_1 > 0$ with direction-dependent interfacial energies are inconsistent with SSY. This is a very undesirable feature given the fundamental importance of the separation of length scales represented by SSY in fracture. To develop cohesive zone models capable of predicting mixed mode failure in *elastic* materials, at least two other choices are possible. The first is to supplement the work function approach with the concept of failure surface in displacement space, as discussed below. The second is to consider non-potential constitutive models.

Two Examples:

Let us consider a pre-exist Mode I plane strain crack in a sample. We assume that the material directly ahead of the crack tip can be modeled by a rigid cohesive zone model (see Figure 10 below) so that the cohesive zone tip exists and it lies inside the specimen.

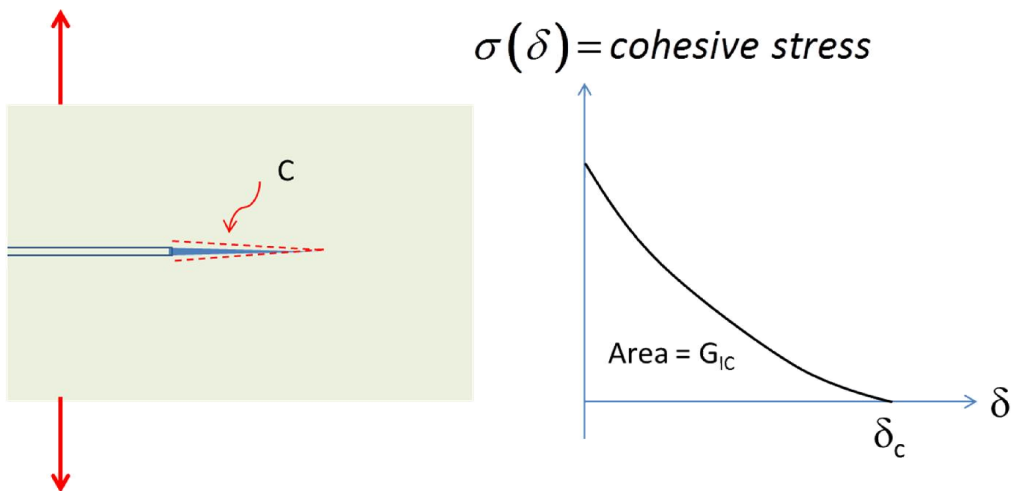


Figure 10a,b: A Rigid cohesive model for a Mode I Crack.

The path of the J integral C (red dotted line) in figure 10a is deformed in such a way so that it just encloses the cohesive zone (note C is an open path, it does not pass the cohesive zone).

$$\begin{aligned}
 J &= \int_C W \underbrace{n_i ds}_0 - \sigma_{ij} n_j u_{i,1} ds = \int_0^{L_c} \sigma(\delta(x_1)) \frac{du_2(x_1, x_2 = 0^+)}{dx_1} dx - \int_0^{L_c} \sigma(\delta(x_1)) \frac{du_2(x_1, x_2 = 0^-)}{dx_1} dx \\
 &= \int_0^{L_c} \sigma(\delta(x_1)) \frac{d\delta}{dx_1} dx_1 = \int_0^{\delta_{tip}} \sigma(\delta) d\delta \quad \delta_{tip} = \delta(x_1 = L_c) \leq \delta_c
 \end{aligned}$$

where L_c is the length of the cohesive zone (determined by requiring bounded stresses at the cohesive zone tip) and

$$\delta = u_2(x_1, x_2 = 0^+) - u_2(x_1, x_2 = 0^-)$$

In particular, $J \neq \frac{K_I^2}{E^*}$, in fact, the K field may not have any region of dominance if the cohesive zone size is large compared with the crack length or other relevant specimen dimensions. Note the area under the σ vs δ curve in Fig. 10b is G_{IC} and crack initiation occurs when the crack opening displacement δ_{tip} at the tip reaches the critical opening displacement δ_c .

A simple example is the Dugdale-Barenblatt model. In mode I, this model states that

$$\sigma(\delta < \delta_c) = \sigma_0 \quad \sigma(\delta \geq \delta_c) = 0$$

The solution of a preexisting Mode I crack in an infinite plane strain/stress body loaded under remote tension $\sigma_{22}(x_1, |x_2| \rightarrow \infty) = \sigma_\infty$ can be found in a review article by Rice [2]. The crack lies occupies $x_1 \in [-a, a], x_2 = 0$. The opening displacement is found to be [2]:

$$\delta_{tip} = \frac{(1+\kappa)\sigma_0 a}{\pi G} \ln \left[1 + \frac{R}{a} \right] \quad (2.58)$$

where R is the size of the cohesive zone (determined by the requirement of bounded stress at the cohesive zone tip) and is given by

$$R = a \left[\sec \left(\frac{\pi \sigma_\infty}{2\sigma_0} \right) - 1 \right] \quad (2.59)$$

For small scale yielding where $R/a \ll 1$, the size of cohesive zone is:

$$R/a \ll 1 \Leftrightarrow \sigma_\infty / \sigma_0 \ll 1 \Rightarrow R/a = \sec \left(\frac{\pi \sigma_\infty}{2\sigma_0} \right) - 1 \approx \frac{1}{2} \left(\frac{\pi \sigma_\infty}{2\sigma_0} \right)^2. \quad (2.60)$$

Note that as the applied tension reaches the cohesive stress, the cohesive zone length goes to infinity. As shown in the example above, the path independence of the J integral tells us that $J = \sigma_0 \delta_{tip}$. Using (2.58), the J integral computed using the elastic fields outside the cohesive zone is

$$J = \frac{(1+\kappa)\sigma_0^2 a}{\pi G} \ln\left[1 + \left(\frac{R}{a}\right)\right] \quad (2.61)$$

The K field in the absence of process zone is $K_I = \sigma_\infty \sqrt{\pi a}$. A comparison with (2.61) shows that

$$J \neq K^2 / E^* \quad (2.62)$$

Equality occurs only where the cohesive zone size becomes *vanishingly* small, that is:

$$J = \frac{(1+\kappa)\sigma_0^2 a}{\pi G} \ln\left[1 + \left(\frac{R}{a}\right)\right] \approx \frac{(1+\kappa)\sigma_0^2 R}{\pi G} \approx \frac{(1+\kappa)\sigma_0^2}{2\pi G} \left(\frac{\pi\sigma_\infty}{2\sigma_0}\right)^2 a = \frac{K^2}{E^*}$$

As explained earlier, the fact that $J \neq K_I^2 / E^*$ implies the existence of high order singularity terms outside the process zone which for the Dugdale model *can be directly verified* by computing the stress field directly ahead of the cohesive zone tip. Also, note that the stresses are bounded everywhere, so the first derivation in this lecture for energy release rate no longer works. Figure 11 below shows a comparison of the *cohesive* (plastic) zone model and the SSY result where plastic (cohesive) zone size goes to zero. For sufficiently large process zone, LEFM overestimates the stress needed to initiate fracture.

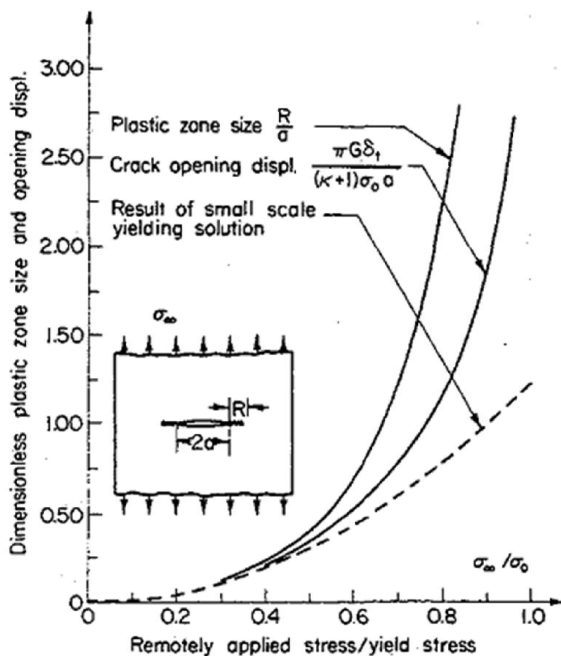


Figure 11: Figure 22 from J. Rice in [2] (see lecture 1), page 266.

References:

- [5] Lake G.J. and A. G. Thomas, Proc. R. Soc. London, Ser. A, 1967, 300, 108)
- [6] Kramer, E.J. (1983), "Crazing in Polymers", in Adv. In Polymer Sci, Kausch H.H. (ed) 52/53: 1- 56
- [7] Needleman, A., (1990), J. Mech. Phys. Solids, vol 38, 289-324.
- [8] Xu X-P, Needleman, A., (1994) J. Mech. Phys. Solids; 42: 1397-1434.
- [9] V. Tvergaard and J. W. Hutchinson, (1992), J. Mech. Phys. Solids, vol 40, 6, 1377-1397.
- [10] V. Tzergaard and J. W. Hutchinson, (1993), J. Mech. Phys. Solids, vol 41, 6, 1119-1135.
- [11] C.Y. Hui, A. Ruina, R. Long and A. Jagota, *J. of Adhesion*, 87,1-52 (2011).

Lecture 4 Introduction to Large Deformation Elastic Fracture Mechanics

Since there is no literature on 3 dimensional theory of cracks in hyper-elastic solids, I will focus on plane theories where the deformation state is completely characterized by two in-plane material coordinates. Because of time limitations, I restrict this lecture to plane strain deformation only. As in lecture 3, the material is assumed to be isotropic, homogeneous, incompressible and Hyper-elastic. The results below are from the paper by

(*) R. A. Stephenson: *J. of Elasticity*, 12, 1, (1982), 65-99 with slight modifications (I have corrected typographical errors and added comments of my own).

Notation: Stephenson's $\overset{\circ}{W} = \Phi$ in my notation. Also, his \bar{n} is denoted by \bar{m} in my notation.

Preliminary: Plane strain theory in large deformation theory:

In plane strain deformation, the out of plane displacement u_3 is assumed to be identically zero. The in plane displacements u_α are assumed to depend only on the in-plane material coordinates x_α , $\alpha=1,2$.

For incompressible Hyperelastic solids, $\lambda_3 = 1$, this implies that $I_1 = \lambda_1^2 + \lambda_1^{-2} + 1 \Rightarrow I_1 = I_2$ so the *work function W is a function of I_1 only*. The deformation gradient tensor, \tilde{F} with respect to an orthonormal basis, can be represented by the matrix

$$F_{ij} \bar{e}_i \bar{e}_j \leftrightarrow \begin{bmatrix} y_{1,1} & y_{1,2} & 0 \\ y_{2,1} & y_{2,2} & 0 \\ 0 & 0 & 1 \end{bmatrix} \Leftrightarrow F_{ij}^T \bar{e}_i \bar{e}_j \leftrightarrow \begin{bmatrix} y_{1,1} & y_{2,1} & 0 \\ y_{1,2} & y_{2,2} & 0 \\ 0 & 0 & 1 \end{bmatrix} \Leftrightarrow F_{ij}^{-T} \bar{e}_i \bar{e}_j = \begin{bmatrix} y_{2,2} & -y_{2,1} & 0 \\ -y_{1,2} & y_{1,1} & 0 \\ 0 & 0 & 1 \end{bmatrix} \quad (4.1)$$

In (4.1), I have used the incompressibility condition

$$J = \det \tilde{F} = y_{1,1} y_{2,2} - y_{1,2} y_{2,1} = 1 \quad (4.2)$$

According to Lecture 3, when the work function is independent of I_2 , the 1st Piola stress is related to the deformation gradient by

$$\tilde{\sigma} = 2\Phi'(I) \tilde{F} - p \tilde{F}^{-T} \quad \text{where } \Phi'(I) = d\Phi / dI \quad (4.3)$$

where p is the pressure require to enforce incompressibility (4.2). Since we are mostly interested in the in-plane fields, we define the 2D deformation gradient and 1st Piola stress tensors by

$$\tilde{F} = F_{\alpha\beta} \bar{e}_\alpha \bar{e}_\beta, \quad \alpha, \beta = 1, 2 \quad \tilde{F} \leftrightarrow \begin{bmatrix} y_{1,1} & y_{1,2} \\ y_{2,1} & y_{2,2} \end{bmatrix} \quad (4.4a)$$

$$\sigma_{\alpha\beta} = 2\Phi'(I) F_{\alpha\beta} - p F_{\alpha\beta}^{-T} \quad (4.4b)$$

where

$$I \equiv \text{tr} \left[\tilde{F}^T \tilde{F} \right] = F_{\alpha\beta} F_{\alpha\beta} \quad (4.4c)$$

Finally, (4.1) and (4.3) imply that the only non-vanishing out of plane component of the 1st Piola stress is

$$\sigma_{33} = 2\Phi'(I) - p. \quad (4.5)$$

Since σ_{33} is independent of the out of plane coordinates, is easy to show that the only non-trivial equilibrium equations are the in-plane ones, and these are, in the reference configuration:

$$\frac{\partial \sigma_{\alpha\beta}}{\partial x_\beta} = 0 \quad (4.6)$$

Note that σ_{33} can be found once the in-plane deformation and the pressure p are determined. In the following, we treat \tilde{F} and $\tilde{\sigma}$ as 2D tensors defined by (4.4a-c).

In lecture 3, I have chosen the origin of the coordinate system to be the same for the reference and deformed configuration. In Stephenson's paper, he shifted the origin of his deformed coordinate system to the deformed crack tip position as shown in figure below. Such a translation does not affect the deformation gradient and all relevant quantities in the calculation.

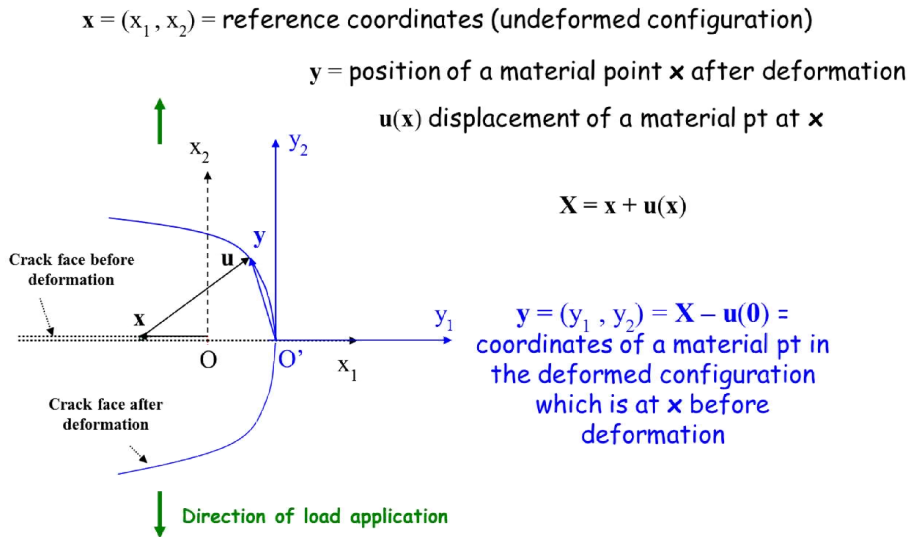


Figure 1: Schematic figure showing the reference and the deformed configuration of a Mode I plane strain crack. Bold letters denote vectors. Note the origin of the deformed coordinate system (y_1, y_2) is located at the deformed crack tip O' .

Governing equations and boundary conditions

Since we are interested in the behavior near the crack tip, the crack can be modeled as semi-infinite with its tip at the origin where $\vec{x} = \vec{0}$. The traction free boundary condition on the crack faces in the reference configuration is:

$$\sigma_{12}(r, \theta = \pm\pi) = \sigma_{22}(r, \theta = \pm\pi) = 0 \quad (4.7)$$

where $(r, \theta = \pm\pi)$ is a polar coordinate system with the origin at $\vec{x} = \vec{0}$, that is, $x_1 = r \cos \theta$, $x_2 = r \sin \theta$, where $-\pi < \theta \leq \pi$. In the following, we make use of the standard formulae:

$$\frac{\partial}{\partial x_1} = \cos \theta \frac{\partial}{\partial r} - \frac{\sin \theta}{r} \frac{\partial}{\partial \theta}, \quad \frac{\partial}{\partial x_2} = \sin \theta \frac{\partial}{\partial r} + \frac{\cos \theta}{r} \frac{\partial}{\partial \theta} \quad (4.8)$$

Using (4.8), the incompressibility constraint (4.2) in polar coordinates is:

$$J = \frac{1}{r} \left(\frac{\partial y_1}{\partial r} \frac{\partial y_2}{\partial \theta} - \frac{\partial y_2}{\partial r} \frac{\partial y_1}{\partial \theta} \right) = 1 \quad (4.9)$$

Substituting (4.4b) into the equilibrium equations (4.6) leads to

$$\frac{\partial \sigma_{\alpha\beta}}{\partial x_\beta} = 0 \Leftrightarrow \frac{\partial \left[2\Phi'(l) F_{\alpha\beta} - p F_{\alpha\beta}^{-T} \right]}{\partial x_\beta} = 0 \quad (4.10a)$$

Using (4.8), (4.4b) and

$$\tilde{F}^{-T} \Leftrightarrow \begin{bmatrix} y_{2,2} & -y_{2,1} \\ -y_{1,2} & y_{1,1} \end{bmatrix} \quad (4.10b)$$

and after some calculations, the equilibrium equations (4.10a) can be written as two coupled nonlinear PDE's (partial differential equations) involving the unknown pressure p and the deformed coordinates y_1, y_2 :

$$\begin{aligned} \frac{\partial p}{\partial r} &= 2\Phi'(l) H_r + 2\Phi''(l) \left[g_{rr} \frac{\partial l}{\partial r} + \frac{g_{r\theta}}{r^2} \frac{\partial l}{\partial \theta} \right] \\ \frac{\partial p}{\partial \theta} &= 2\Phi'(l) H_\theta + 2\Phi''(l) \left[g_{r\theta} \frac{\partial l}{\partial r} + \frac{g_{\theta\theta}}{r^2} \frac{\partial l}{\partial \theta} \right] \end{aligned} \quad (4.11a,b)$$

where $\Phi''(l) = d^2\Phi / dl^2$ and

$$g_{rr} = \frac{\partial y_\alpha}{\partial r} \frac{\partial y_\alpha}{\partial r}, \quad g_{r\theta} = \frac{\partial y_\alpha}{\partial r} \frac{\partial y_\alpha}{\partial \theta}, \quad g_{\theta\theta} = \frac{\partial y_\alpha}{\partial \theta} \frac{\partial y_\alpha}{\partial \theta} \quad (4.11c)$$

$$H_r = \frac{\partial y_\alpha}{\partial r} \nabla^2 y_\alpha \quad H_\theta = \frac{\partial y_\alpha}{\partial \theta} \nabla^2 y_\alpha \quad (4.11d)$$

$$I = g_{rr} + \frac{1}{r^2} g_{\theta\theta} \quad (4.11e)$$

The use of summation convention of summing over repeated indices is used unless specified otherwise. Using (4.4b), (4.10b) and (4.8), the boundary conditions (4.7) can be written as:

$$\begin{aligned} \left[2\Phi'(I) \frac{\partial y_1}{\partial \theta} + rp \frac{\partial y_2}{\partial r} \right]_{\theta=\pm\pi} &= 0 \\ \left[2\Phi'(I) \frac{\partial y_2}{\partial \theta} - rp \frac{\partial y_1}{\partial r} \right]_{\theta=\pm\pi} &= 0 \end{aligned} \quad (4.12a,b)$$

It can be shown using (4.11c) and (4.9) that (4.12a,b) is equivalent to (e.g. by multiplying (4.12a) by $\frac{\partial y_2}{\partial \theta} \Big|_{\theta=\pm\pi}$ and (4.12b) by $\frac{\partial y_1}{\partial \theta} \Big|_{\theta=\pm\pi}$ and subtracting the resulting expressions leads to 4.13b),

$$p \Big|_{\theta=\pm\pi} = \frac{2\Phi'(I)}{g_{rr}} \Big|_{\theta=\pm\pi} = \frac{2\Phi'(I)g_{\theta\theta}}{r^2} \Big|_{\theta=\pm\pi}, \quad g_{r\theta}(r, \theta = \pm\pi) = 0 \quad (4.13a,b)$$

The three PDE's ((4.9) and (4.11a,b)) and the boundary conditions (4.13a,b) allows one to solve for the unknown pressure and the deformed positions y_1, y_2 .

The only thing left is to specify the work or energy density function $W = \Phi(I)$. Since one is interested in asymptotic behavior where the local fields are unbounded, Stephenson assumes that the behavior of the energy density function for large I has the form:

$$\Phi(I \rightarrow \infty) = AI^n + BI^{n-1} + o(I^{n-1}) \quad (4.14)$$

where n is a positive real number and can be interpreted as a hardening parameter¹. The constants A and B has units of stress, A can be interpreted as a reference modulus. For example, for a Mooney-Rivlin material, the strain energy density in plane strain deformation is the same as a neo-Hookean solid which is given by

$$\Phi(I) = \frac{\mu}{2}(I-2) \quad (4.15)$$

For this special case (4.4) is valid for all levels of deformation with $n=1, A = \mu/2, B = -\mu$. Note for Mooney-Rivlin solid, $\Phi''(I) = 0$, leading to considerable simplification of (4.11a,b).

¹ For a stable material, $n > 1/2$, see Stephenson's paper (*) for a detailed discussion.

Key assumption:

The key assumption is that the dominant solution of (4.9) and (4.11a,b) as $r \rightarrow 0$ is *separable*, that is:

$$y_1 = r^{m_1} U_1(\theta), \quad y_2 = r^{m_2} U_2(\theta), \quad p = r^l P(\theta) \quad \text{as } r \rightarrow 0 \quad (4.16a,b,c)$$

where m_α, l , are unknown constants. The angular functions U_α, P are also unknown. To allow for singular fields with bounded displacements, the unknown constants m_α are restricted to satisfy:

$$1 > \min\{m_1, m_2\} = m > 0. \quad (4.17)$$

Key observation

An important observation by Stephenson [*] is the following: Suppose there exist a solution $\{\bar{y}, \bar{\sigma}, p\}$ that satisfies the field equations (4.2), (4.3) and (4.6) as well as the traction free boundary conditions imposed on the crack faces (4.7), then $\{\tilde{Q}\bar{y}, \tilde{Q}\bar{\sigma}, p\}$ is also a solution of the crack problem, where \tilde{Q} is *any* constant proper orthogonal tensor (that is, $\det \tilde{Q} = 1$). With respect to an orthonormal basis, the matrix of \tilde{Q} must have the form:

$$\tilde{Q} \leftrightarrow \begin{bmatrix} \cos \phi & -\sin \phi \\ \sin \phi & \cos \phi \end{bmatrix} \quad \phi \in [0, 2\pi) \quad (4.18)$$

To see this, note that the equilibrium equation (4.3) is satisfied by $\tilde{Q}\bar{\sigma}$, since \tilde{Q} is a constant tensor. The deformation gradient due to the application of \tilde{Q} to \bar{y} is $\tilde{Q}\tilde{F}$. Since the work function depends only on the invariants of the Cauchy-Green tensor $\tilde{F}^T \tilde{F}$, it is unaffected by a rigid body rotation, that is

$$(\tilde{Q}\tilde{F})^T (\tilde{Q}\tilde{F}) = (\tilde{F}^T \tilde{Q}^T) (\tilde{Q}\tilde{F}) = \tilde{F}^T \tilde{F}.$$

This means that

$$\tilde{\sigma} = 2\Phi'(I)\tilde{F} - p\tilde{F}^{-T} \Leftrightarrow \tilde{Q}\bar{\sigma} = 2\Phi'(I)\tilde{Q}\tilde{F} - p(\tilde{Q}\tilde{F})^{-T} \quad (4.19)$$

So $\tilde{Q}\bar{\sigma}$ satisfies the constitutive model. Finally, the traction caused by $\tilde{Q}\bar{\sigma}$ on the crack faces is

$$[\tilde{Q}\bar{\sigma} \cdot \bar{e}_2]_{\theta=\pm\pi} = \begin{bmatrix} \cos \phi & -\sin \phi \\ \sin \phi & \cos \phi \end{bmatrix} \underbrace{\begin{pmatrix} \sigma_{12}(r, \theta=\pm\pi) \\ \sigma_{22}(r, \theta=\pm\pi) \end{pmatrix}}_{\bar{0}} = \bar{0} \quad \text{QED}$$

Let us apply \tilde{Q} to the displacement field specified by (4.16a,b), we have

$$\bar{y}^* \equiv \tilde{Q}\bar{y} = \tilde{Q}(y_\alpha \bar{e}_\alpha) \Rightarrow \begin{pmatrix} y_1^* \\ y_2^* \end{pmatrix} = r^{m_1} U_1(\theta) \begin{pmatrix} \cos \varphi \\ \sin \varphi \end{pmatrix} + r^{m_2} U_2(\theta) \begin{pmatrix} -\sin \varphi \\ \cos \varphi \end{pmatrix} + \text{higher order terms}$$

Hence it is always possible to choose a suitable rotation, i.e., φ so that

$$y_\alpha^* = r^m U_\alpha^*(\theta) + o(r^m) \quad r \rightarrow 0 \quad (4.20)$$

This means that there is no loss in generality to assume that both deformed coordinates has the same power exponent m , i.e.,

$$y_\alpha = r^m U_\alpha(\theta) + o(r^m) \quad r \rightarrow 0 \quad (4.21)$$

Note that the solution given by (4.21) in general will not satisfied the symmetric conditions imposed by a *Mode I* crack, that is,

$$y_1(x_1, x_2) = y_1(x_1, -x_2) \quad \& \quad y_2(x_1, -x_2) = -y_2(x_1, x_2) \quad (4.22)$$

Therefore, in order to obtain local *Mode I* fields, it is necessary to consider higher order terms of the expansion of y_α since $U_1(\theta)$ may have to be identical zero in order to satisfy (4.22). In particular, there is no guarantee that such symmetric solution should exist. Indeed, Stephenson showed that there is no solution that satisfies the *Mode II* or *anti-symmetry* condition:

$$y_1(x_1, x_2) = -y_1(x_1, -x_2) \quad \& \quad y_2(x_1, -x_2) = y_2(x_1, x_2) \quad (4.23)$$

In short, there is no *Mode II* in the nonlinear theory!

In summary, to consider the local crack tip field in a plane strain incompressible hyperelastic solid, one assumes a local solution of the form:

$$y_\alpha = r^m U_\alpha(\theta) + r^{m'} V_\alpha(\theta) + \text{higher order terms} \quad m' > m \quad (4.24)$$

The general procedure consist of substituting (4.24) into the nonlinear governing equations and match terms of equal order, as well as requiring these solutions to satisfy the traction free boundary conditions. In theory, the procedure is straightforward. However, in practice, these calculations can be extremely messy and tricky and will not be presented here (many details can be found in Stephenson [*]). In this lecture I summarize the main relevant results which is for $n = 1$ and for large n ($n \geq 7/2$)

n = 1

This case corresponds to the Mooney-Rivlin solid. Stephenson's solution ((4.25) in his paper [*]) is:

$$\begin{aligned}
y_1 &= a_1 r^{1/2} \sin(\theta/2) + \frac{r}{a^2} [a_1 b_1 \cos \theta - a_2 b_2 \sin^2(\theta/2)] + O(r^{3/2}) \\
y_2 &= a_2 r^{1/2} \sin(\theta/2) + \frac{r}{a^2} [a_1 b_2 \sin^2(\theta/2) + a_2 b_1 \cos \theta] + O(r^{3/2}) \\
\rho &= -2 \frac{\mu b_2}{a^2} r^{1/2} \cos(\theta/2) + O(r)
\end{aligned} \tag{4.25a,b,c}$$

where a_α, b_α are arbitrary constants that cannot be determined by local analysis (it depends on the specimen geometry and the loading conditions). Also, a in (4.25c) is defined by

$$a = \sqrt{a_1^2 + a_2^2} > 0. \tag{4.25d}$$

Although Stephenson does not mention this in his paper, the result given by (4.25a,b) gives the following result if $a_\alpha \neq 0$. On the crack faces, $\theta = \pm\pi$, we have, as $r \rightarrow 0$,

$$y_1(\theta = \pm\pi) = \pm a_1 r^{1/2}, \quad y_2(\theta = \pm\pi) = \pm a_2 r^{1/2} \Rightarrow y_2 / y_1 = a_2 / a_1 \tag{4.26}$$

Let us suppose $a_1 < 0$, then $y_1 > 0$ for the lower crack face so it must undergo very large rotation - the crack faces open into a straight line locally.

Note that (4.25a,b) cannot satisfy the Mode I symmetry conditions (4.22) unless

$$a_1 = 0, a = |a_2|, b_1 = 0 \tag{4.27a}$$

Thus, for Mode I, we have

$$\begin{aligned}
y_1 &= -\frac{r}{a} [b_2 \sin^2(\theta/2)] + O(r^{3/2}) \\
y_2 &= a_2 r^{1/2} \sin(\theta/2) + O(r^{3/2})
\end{aligned} \tag{4.27b,c}$$

There is but one problem with the above solution, eqn. (4.27b) predicts that $y_1 = 0$ directly ahead of the crack tip. While we expect $y_2 = 0$ directly ahead of the crack tip, y_1 should not. In other words, the mapping between the deformed and undeformed configuration given by (4.27b,c) is not one-one. To remedy this situation, a higher order expansion for y_1 is needed. This was done by Stephenson (see (4.37) in his work). His result is

$$\begin{aligned}
y_1 &= -\frac{b_2}{a} r \sin^2(\theta/2) + \frac{1}{a} r^{3/2} \left[\frac{4}{3} \cos^3(\theta/2) + 4 \sin^2(\theta/2) \cos(\theta/2) \right] + O(r^2) \\
y_2 &= a r^{1/2} \sin(\theta/2) + \frac{1}{a} r^{3/2} \left[c_1 \sin(3\theta/2) - \frac{b_2^2}{2a^2} \sin(\theta/2) \right] + O(r^2), \quad |a_2| = a
\end{aligned} \tag{4.27d}$$

Thus,

$$y_1(r \rightarrow 0, \theta = 0) = \frac{4}{3a} r^{3/2} + O(r^2) \quad (4.27e)$$

As expected, in Mode I the crack opens up symmetrically, that is, at $\theta = \pm\pi/2$, $-y_1 = cr$, where we assume $c = \frac{b_2}{a} > 0$. In this case, we have $y_2 = \pm a_2 r^{1/2}$ for the upper and lower crack faces, thus,

$$y_2 = \pm a_2 c^{1/2} |y_1|^{1/2} \quad (4.27f)$$

Thus, the crack opening displacement of a *Mode I crack* for a Mooney-Rivlin or Neo-hookean solid behaves in the same way as a linear elastic material. However, there is no Mode II !

The case of $n \geq 7/2$

A well-known difficulty with the Mooney-Rivlin model is that it under-predicts strain hardening. This will affect the asymptotic behavior of the crack tip fields. Therefore, it is reasonable to consider the limit of very large n in the model, it is for this reason that I have not included the results for $1 < n < 7/2$. For these cases Stephenson only gives the dominant solution for y_α in his paper (see (3.104) in [*]), where

$$\begin{aligned} y_1 &= -\frac{1}{a} r^{2-m} H(\theta) + o(r^{2-m}), & m &= 1 - \frac{1}{2n} \\ y_2 &= -ar^m U(\theta) + \frac{1}{a} r^{2-m} \chi(\theta) + o(r^{2-m}) \end{aligned} \quad (4.28a,b)$$

Here

$$\begin{aligned} U(\theta) &= \sin(\theta/2) \sqrt{1 - \frac{2\kappa^2 \cos^2(\theta/2)}{1+\omega}} [\omega + \kappa \cos \theta]^{\kappa/2}, \\ \omega &= \sqrt{1 - \kappa^2 \sin^2(\theta/2)}, \quad \kappa = \frac{n-1}{n} \end{aligned} \quad (4.28c,d,e)$$

$$H(\theta) = -\frac{n^{5/2}}{m^2} [\omega + \kappa \cos \theta]^{2-m} \left[\frac{m}{2-m} F\left(1/2 - 1/m, 1/2; 3/2 - 1/m; \cos^2 \xi_0\right) - \kappa \sin \xi_0 \right]$$

where F stands for the Hypergeometric function (see page 556 in Handbook of Mathematical Functions, by Abramowitz, M and Stegun I, A., for definition and properties of these functions), $m = 1 - \frac{1}{2n}$ and

$$\cos \xi_0 = \frac{1}{n\sqrt{2}} \frac{\sqrt{1 + \kappa \sin^2 \theta - \omega \cos \theta}}{\omega + \kappa \cos \theta}, \quad \theta \in [0, \pi] \quad (4.28f)$$

Finally,

$$\chi(\theta) = c_2 [\omega + \kappa \cos \theta]^{2-m} \left[\frac{1 + \kappa \sin^2 \theta - \omega \cos \theta}{n^2 [\omega + \kappa \cos \theta]^2} - 1 \right] \quad (4.28g)$$

Note, since $\omega(\theta=0)=1$ (see 4.28d), $\cos \xi_0 = 0$ at $\theta=0$. In addition, by virtue of (4.28f), H is an even function of θ , so y_1 is an even function of x_2 . Also, U is an odd function of x_2 . Hence if we take the constant $c_2 = 0$ in (4.28g), we will have the dominant terms for a Mode I crack:

$$\begin{aligned} y_1 &= -\frac{1}{a} r^{2-m} H(\theta) + o(r^{2-m}), & m &= 1 - \frac{1}{2n} \\ y_2 &= ar^m U(\theta) + o(r^{2-m}) \end{aligned} \quad (4.28)$$

For *Mode I* loading, according to (4.28a,b), the crack faces are carried into curves in the (y_1, y_2) space given by

$$\begin{aligned} y_1 &= -\frac{1}{a} r^{2-m} H(\pm\pi) \Rightarrow \left[\frac{a}{H(\pm\pi)} (-y_1) \right]^{1/(2-m)} = r & m &= 1 - \frac{1}{2n} \\ y_2 &= ar^m U(\pm\pi) \Rightarrow y_2 = \pm k(n) a^{\frac{2}{2-m}} |y_1|^{\frac{2n-1}{2n+1}}, & y_1 &< 0, \end{aligned} \quad (4.29)$$

Stephenson has shown that $H(\pm\pi) > 0$, therefore, $k(n) > 0$. Note that for very large n , Eq. 4.29 implies that the deformed crack faces are *almost* flat. Thus, strain hardening gives crack opening displacements that are substantially different from prediction of linear elasticity. In fact, Stephenson [*] shown that the crack profile for general loading is still given by (4.29) (see (5.3) in [*]), so the crack will always open, there is no Mode II).

Stresses

The 1st Piola stresses in the reference coordinate (r, θ) can be worked out using (4.4b) and the asymptotic expansion of y_α given above. Likewise, the asymptotic true stress fields can be obtained using

$$\tau_{\alpha\beta} = 2\Phi'(I) F_{\alpha\gamma} F_{\beta\gamma} - p\delta_{\alpha\beta} \quad (4.30a)$$

or

$$\tilde{\tau} = \tilde{\sigma} \tilde{F}^T \quad (4.30a)$$

Let us consider the simple case of $n = 1$, for Mode I, using the dominant terms in (4.37) leads to

$$\begin{aligned}\sigma_{11}(r, \theta) &= \frac{\mu b_2}{a} \\ \sigma_{12}(r, \theta) &= 0 + \text{higher order terms} \\ \sigma_{21}(r, \theta) &= -\frac{\mu a}{2\sqrt{r}} \sin(\theta/2) \\ \sigma_{22}(r, \theta) &= \frac{\mu a}{2\sqrt{r}} \cos(\theta/2)\end{aligned}\quad \text{Mode I, } n=1 \quad (4.31a-d)^2$$

The true stresses are:

$$\begin{aligned}\tau_{11}(r, \theta) &= \mu (b_2/a)^2 \sin^2(\theta/2) \\ \tau_{12}(r, \theta) &= \frac{\mu b_2}{2} r^{-1/2} \sin(\theta/2) \\ \tau_{22}(r, \theta) &= \frac{\mu a^2}{4r}\end{aligned}\quad \text{Mode I, } n=1 \quad (4.32a-c)$$

- Note that the three components of the stresses at the crack tip have different orders of singularity. In Mode I, the normal stress τ_{22} dominates. Therefore, the stress state at the crack tip is that of uniaxial tension.
- This means that the stress state directly ahead of the crack tip is not *hydrostatic* which is predicted by linear theory. Indeed, notice that (4.32a) states that $\tau_{11}(r, \theta)$ is bounded everywhere, in particular, $\tau_{11}(r \rightarrow 0, \theta = 0) = 0$ whereas in linear elasticity

$$\tau_{11}(r \rightarrow 0, \theta = 0) = \tau_{22}(r \rightarrow 0, \theta = 0) = \frac{K_I}{\sqrt{2\pi r}} .$$

- Note that the true stresses, expressed in terms of the *material coordinate system* (r, θ) are *separable*.

Mode I, $n > 7/2$

For a Mode I crack, the true stresses are (see Stephenson, 5.9 and 5.11)

$$\begin{aligned}\tau_{11}(r, \theta) &= o\left(r^{-1+(1/n)}\right) \\ \tau_{12}(r, \theta) &= Ak_{12}r^{-1+(1/n)} [\omega + \kappa \cos \theta]^{-1/(2n)} \cos \xi_0, \quad k_{12} \equiv 4b_0 a^{2n-1} m^{2n} n^{(3/2)-n} \\ \tau_{22}(r, \theta) &= Ak_{22}r^{-1} [\omega + \kappa \cos \theta]^{-1}, \quad k_{22} = 2a^{2n} m^{2n} n^{1-n}\end{aligned}\quad (4.33a-c)$$

Recall that A (see 4.14) can be regarded as a reference modulus, the constants b_0 and a cannot be determined by local analysis as they depend on the applied loading and specimen geometry.

² This result given by (4.31a-d) is not in Stephenson. It is derived using his results.

Just as the case of $n = 1$, the near tip stresses in Mode I is still dominated by the normal component of the stress tensor. However, the differences between different stress components become much smaller as the hardening parameter n increases. Therefore, hardening recovers the hydrostatic state of stress near the crack tip. The near tip field is controlled by two parameters b_0 and a (instead of a single parameter in LEFM). However, the dominant field (which contributes to the J integral or energy release rate) depends only on the parameter a .

Stress in deformed coordinates

In most papers on the subject, the stresses (true or 1st Piola) are expressed in terms of the material coordinates x_α . A more practical way is to express these local fields in the deformed coordinates y_α . For example, one describes the shape of the deformed crack by specifying how y_2 varies with y_1 . As I shall demonstrate below, the stresses expressed in terms of the deformed coordinates are not separable, and exhibits interesting behavior that are not readily seen when they are expressed in material coordinates. Take for example, a Mode I crack with $n = 1$, where the true stresses are given by (4.32a-c). Let us look at the component of stress that gives the highest singularity τ_{22} . When expressed in material coordinates,

$$\tau_{22}(r, \theta) = \frac{\mu a^2}{4r} \quad (4.34)$$

which is independent of θ . To express τ_{22} in the deformed coordinates, we need to invert the local mapping between the undeformed and the deformed configurations which is given by (4.27a,b). Note that if we ignore the higher order term $r^{3/2}$ in (4.27a), then the mapping is not invertible. Therefore, we have kept this additional term, that is,

$$\begin{aligned} y_1 &= -\frac{r}{a} b_2 \sin^2(\theta/2) + \frac{1}{a} r^{3/2} \left[\frac{4}{3} \cos^3(\theta/2) + 4 \sin^2(\theta/2) \cos(\theta/2) \right] \\ y_2 &= a r^{1/2} \sin(\theta/2) \end{aligned} \quad (4.35a,b)$$

Equation (4.34) requires us to express r in terms of y_1, y_2 which I have not been able to do. Such close form expression, if exist, are not separable.

To gain insight, let us first examine *directly* ahead of the crack tip, at $\theta = 0$. From (4.25b), we see that $y_2 = 0$, thus, *directly* ahead of the crack tip,

$$y_1 = \frac{4}{3a} r^{3/2} \quad \theta = 0 \Rightarrow y_2 = 0, \quad (4.36)$$

Substituting (4.36) into (4.34), we obtain

$$\tau_{22}(y_1, y_2 = 0) = \frac{\mu a^2}{4} \left(\frac{4}{3a y_1} \right)^{2/3} = \frac{\mu a^2}{4} \left(\frac{4}{3a \rho} \right)^{2/3} \quad y_1 > 0 \quad (4.37a)$$

where I have introduced the polar coordinate system (ρ, ϕ) in the deformed configuration, where

$$y_1 = \rho \cos \phi, y_2 = \rho \sin \phi, \quad -\pi < \phi \leq \pi \quad (4.37b)$$

Eq. (4.37a) implies that the stress singularity directly ahead of the crack tip is reduced when expressed in the deformed coordinates. Note that this result is valid only at $\theta = 0$. On the other hand, let us approach the crack tip from the upper crack face, that is, $\theta \rightarrow \pi$, (4.35a,b) implies that

$$|y_2| \gg |y_1| \Rightarrow \rho = y_2, \phi \rightarrow \pi/2 \Rightarrow r = (\rho/a)^2 \quad (4.38)$$

This means that,

$$\tau_{22}(\rho, \phi = \pi/2) = \frac{\mu a^2}{4} \left(\frac{a}{\rho} \right)^2 \quad (4.39)$$

The singularity in τ_{22} is much higher as we approach the crack tip from the crack faces.

For a Mode-I crack in a neo-Hookean material, the asymptotic solution of crack tip deformation field is given in Stephenson (*). Using eq. (4.27d) above, we have, after normalizing y_1, y_2 and r by a^2 :³

$$\frac{y_1}{a^2} = -\left(\frac{b_2}{a}\right)\left(\frac{r}{a^2}\right)\sin^2\left(\frac{\theta}{2}\right) + \left(\frac{r}{a^2}\right)^{3/2} \left(4\sin^2\left(\frac{\theta}{2}\right)\cos\left(\frac{\theta}{2}\right) + \frac{4}{3}\cos^3\left(\frac{\theta}{2}\right)\right), \quad (4.40a)$$

$$\frac{y_2}{a^2} = \left(\frac{r}{a^2}\right)^{1/2} \sin\left(\frac{\theta}{2}\right) + \left(\frac{r}{a^2}\right)^{3/2} \left(c_1 \sin^3\left(\frac{\theta}{2}\right) - \frac{1}{2}\left(\frac{b_2}{a}\right)^2 \sin\left(\frac{\theta}{2}\right)\right), \quad (4.40b)$$

To plot the deformation mapping from the undeformed configuration (r, θ) to the deformed configuration (y_1, y_2) , we assume $c_1=1$ and $b_2/a = 1$. The mapping is shown below for $0 \leq r \leq 0.1$ and $0 \leq \theta \leq \pi$.

³ C.Y. Hui is grateful to Prof. Rong Long at the University of Alberta, who kindly provide the numerical calculations and graphs below.

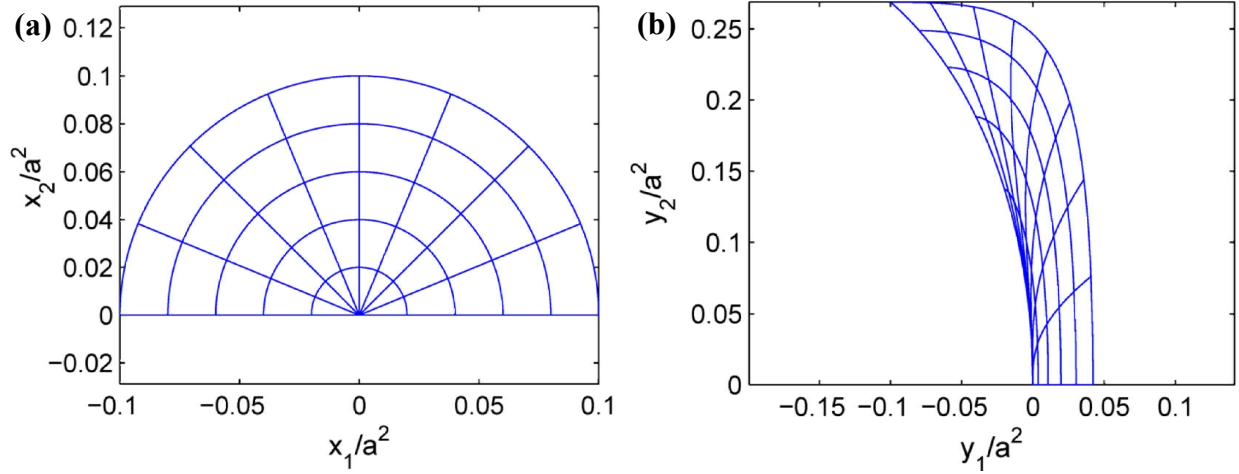


Figure 2. Mapping of the asymptotic crack tip field: (a) a “mesh” in undeformed configuration; the crack surface lies at $x_2=0$ and $x_1<0$; (b) deformed “mesh” calculated using (4.40a,b).

2. True stress field

Again using the solution of Stephenson (*), the true stress components expressed in terms of the undeformed coordinates (r,θ) are:

$$\frac{\tau_{11}}{\mu} = \left(\frac{b_2}{a}\right)^2 \sin^2\left(\frac{\theta}{2}\right), \quad (4.41a)$$

$$\frac{\tau_{12}}{\mu} = -\frac{1}{2}\left(\frac{b_2}{a}\right)\left(\frac{r}{a^2}\right)^{-1/2} \sin\left(\frac{\theta}{2}\right) + \sin\theta \cos\theta, \quad (4.41b)$$

$$\frac{\tau_{22}}{\mu} = \frac{1}{4}\left(\frac{r}{a^2}\right)^{-1/2} + \left(\frac{3}{2}c_1 \cos\theta - \frac{1}{2}\left(\frac{b_2}{a}\right)^2 \left(\frac{1}{2} - \sin\frac{\theta}{2} \sin\frac{3\theta}{2}\right)\right). \quad (4.41c)$$

The color contour of the three stress components in the deformed coordinates, computed using the mapping (4.40a,b) are given below.

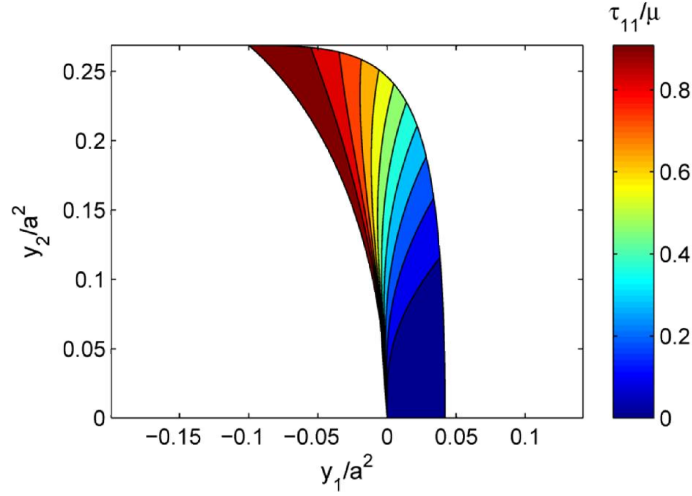


Figure 3 Contour plot of the normalized true stress τ_{11}/μ

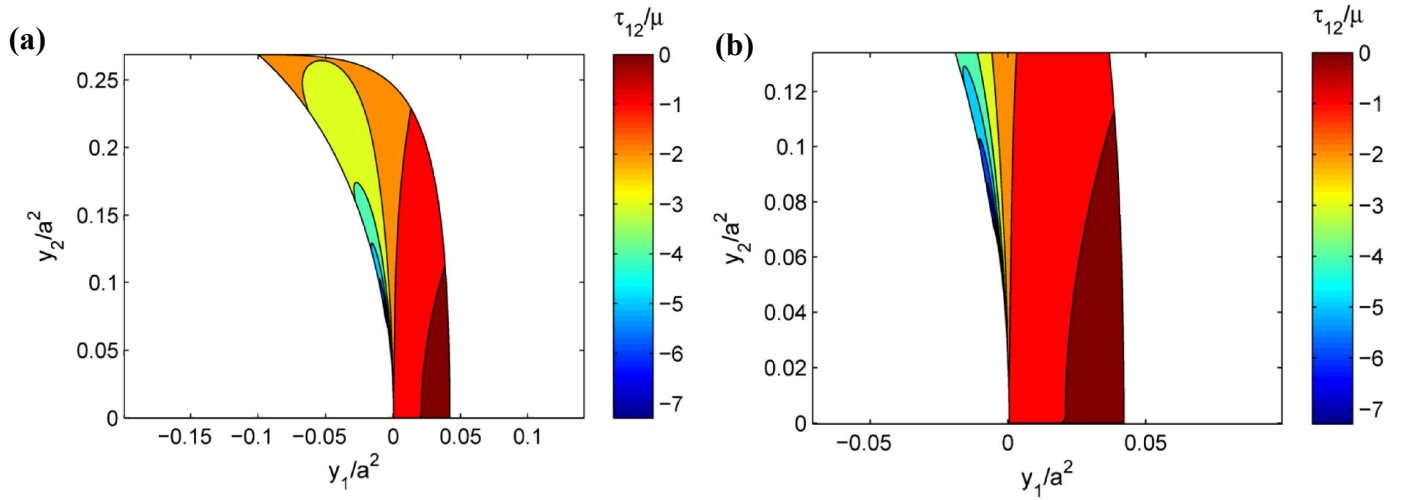


Figure 4 (a) Contour plot of the normalized true stress τ_{12}/μ ; (b) zoom-in view of the crack tip.

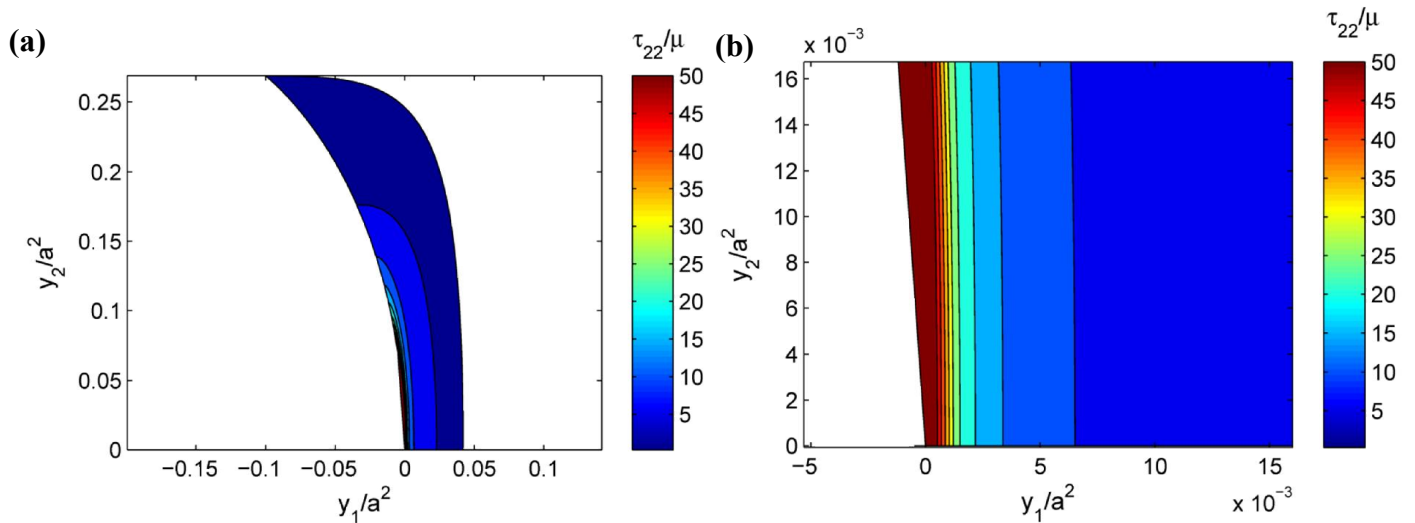


Figure 5 (a) Contour plot of the normalized true stress τ_{22}/μ ; (b) zoom-in view of the crack tip.